# CZECH TECHNICAL UNIVERSITY IN PRAGUE

## Faculty of Mechanical Engineering

## Department of Process Engineering

# CFD Simulation of Heat Transfer in an Agitated Vessel

Master Thesis

**by**

**Luis Alberto Torres Tapia**

2019

Supervisor: Ing. Karel Petera, Ph.D.

# Thesis Assignment

**CTU** CZECH TECHNICAL UNIVERSITY IN PRAGUE

## MASTER'S THESIS ASSIGNMENT

### I. Personal and study details

| | | | |
|---|---|---|---|
| Student's name: | **Torres Tapia Luis Alberto** | Personal ID number: | **476496** |
| Faculty / Institute: | **Faculty of Mechanical Engineering** | | |
| Department / Institute: | **Department of Process Engineering** | | |
| Study program: | **Mechanical Engineering** | | |
| Branch of study: | **Process Engineering** | | |

### II. Master's thesis details

Master's thesis title in English:

**CFD analysis of heat transfer in agitated vessel with draft tube**

Master's thesis title in Czech:

**CFD analýza přestupu tepla v míchané nádobě se středovou trubkou**

Guidelines:

- Make a basic literature research concerning the heat transfer in agitated vessels.
- Perform an analysis to find a proper length of the simulated time interval with the given geometry and mesh.
- Use MRF approach in ANSYS CFD, compare several turbulence models in the simulations and choose a suitable model for the consequent simulations.
- Perform numerical simulations of heat transfer in the agitated vessel with the draft tube for different rotation speeds and evaluate heat transfer coefficients.
- Summarize the methodology used in the thesis and propose possible improvements of the solution procedure.

Bibliography / sources:

According to the recommendation of the supervisor.

Name and workplace of master's thesis supervisor:

**doc. Ing. Karel Petera, Ph.D.,   Department of Process Engineering,   FME**

Name and workplace of second master's thesis supervisor or consultant:

Date of master's thesis assignment: **23.04.2019**    Deadline for master's thesis submission: **07.06.2019**

Assignment valid until: _____

| doc. Ing. Karel Petera, Ph.D. | prof. Ing. Tomáš Jirout, Ph.D. | prof. Ing. Michael Valášek, DrSc. |
|---|---|---|
| Supervisor's signature | Head of department's signature | Dean's signature |

### III. Assignment receipt

The student acknowledges that the master's thesis is an individual work. The student must produce his thesis without the assistance of others, with the exception of provided consultations. Within the master's thesis, the author must state the names of consultants and include a list of references.

| 3 0 -04- 2019 | |
|---|---|
| Date of assignment receipt | Student's signature |

# Annotation sheet

**Name:** Luis Alberto

**Surname:** Torres Tapia

**Title Czech:** CFD analýza přestupu tepla v míchané nádobě se středovou trubkou

**Title English:** CFD analysis of heat transfer in agitated vessel with draft tube

**Scope of work:**     number of pages: 58

                            number of figures: 16

                            number of tables: 14

                            number of appendices: 1

**Academic year:** 2018/2019

**Language:** English

**Department:** Process Engineering

**Specialization:** Process Engineering

**Supervisor:** Ing. Karel Petera, Ph. D.

**Submitter:** Czech Technical University in Prague. Faculty of Mechanical Engineering, Department of Process Engineering

**Annotation - English:** - Make a basic literature research concerning the heat transfer in agitated vessels. - Perform an analysis to find a proper length of the simulated time interval with the given geometry and mesh. - Use MRF approach in ANSYS CFD, compare several turbulence models in the simulations and choose a suitable model for the consequent simulations. - Perform numerical simulations of heat transfer in the agitated vessel with the draft tube for different rotation speeds and evaluate heat transfer coefficients. - Summarize the methodology used in the thesis and propose possible improvements of the solution procedure.

**Keywords:** agitated vessel, heat transfer, energy balance, SST k-ω, dimensionless distance

**Utilization:** For Department of Process Engineering, Czech Technical University in Prague.

## Declaration

I hereby declare that I have completed this thesis entitled CFD Simulation of Heat Transfer in an Agitated Vessel with a draft tube independently with consultations with my supervisor and I have attached a full list of used references and citations.

I do not have a compelling reason against the use of the thesis within the meaning of Section 60 of the Act No.121/2000 Coll., on copyright, rights related to copyright and amending some laws (Copyright Act).

In Prague, Date: ...................                                    .........................
                                                                        Name and Surname

# Acknowledgements

This project is dedicated to my parents who have been my support and example since I was a kid and to my sister and niece, who are part of my life.

My sincere gratitude to my thesis supervisor, Ing. Karel Petera, Ph.D., who always was there to guide me and solve my doubts. I appreciate all your teachings during the courses and the development of my thesis.

Finally, I would like to thanks to all my friends that I have met during my master in Prague. They have done the experience outstanding.

# Abstract

Computational fluid dynamics (CFD) analysis of heat transfer in agitated vessel with a draft tube was performed by using Moving Reference Frame (MRF) approach and SST k-ω model in ANSYS Fluent. First, simulations for different time intervals (0-200 seconds) were run to compare the heat transfer coefficient from Fluent and energy balance. In addition, a proper simulation time interval was found for the following set of simulations. Next, simulations for different rotational speeds were performed, applying SST k-ω model with different options activated, in order to compare which method fits better with published correlations. As a result, SST k-ω model with Production Limiter and Production Kato-Launder was used for the subsequent simulations for different position of the draft tube with respect to the vessel bottom ($h/d$= 0,5 and 0,25). A correlation describing Nusselt number in terms of the Reynolds number, Prandtl number and dimensionless distance ($h/d$) was obtained and was compared with published correlations.

**Keywords**:  agitated vessel, heat transfer, energy balance, SST k-ω, dimensionless distance

# Table of Contents

# List of Tables

# List of Figures

# Nomenclature

## General nomenclature

| | |
|---|---|
| $a$ | thermal diffusivity ($m^2$ $s^{-1}$) |
| $C$ | precorrelation factor for Nu (-) |
| $C_1$ | model parameter (-) |
| $c_p$ | specific heat ($J$ $kg^{-1}$ $K^{-1}$) |
| $d$ | characteristic length, inner diameter of the draft tube (m) |
| $d_m$ | diameter of impeller (m) |
| $G_c$ | geometry correction factor (-) |
| $G_u$ | axial flux of axial momentum ($kg$ $m^2$ $s^{-1}$) |
| $G_w$ | axial flux of tangential momentum ($kg$ $m^2$ $s^{-1}$) |
| $h$ | distance of draft tube from bottom (m) |
| $m$ | mass (kg) |
| $n$ | rotational speed of impeller ($s^{-1}$) |
| $N_Q$ | dimensionless pumping capacity (-) |
| Nu | Nusselt Number (-) |
| $p,q,s$ | general exponents for dimensionless numbers |
| Pr | Prandtl Number (-) |
| $q_w$ | heat flux ($W$ $m^{-2}$) |
| $\dot{Q}$ | hear transfer rate (W) |
| Re | Reynolds Number for a jet (-) |

$Re_m$    Reynolds Number for a mixing system (-)

$S$    heat transfer area ($m^2$)

Sw    Swirl number (-)

$T$    temperature of agitated liquid (K)

$T_b$    final temperature of the batch (K)

$T_f$    final temperature of agitated liquid (K)

$T_o$    initial temperature of agitated liquid (K)

$T_{ref}$    reference temperature of the liquid (K)

$T_w$    wall temperature (K)

$U$    mean velocity in the axial direction (m s$^{-1}$)

$W$    tangential velocity (m s$^{-1}$)

$W^*$    dimensionless maximum tangential velocity at the outlet of the draft tube

Vi    Sieder-Tate factor for temperature dependency (-)

$\Delta T$    temperature difference (K)

$\Delta t$    time interval (s)

$\alpha$    heat transfer coefficient (W m$^{-2}$ K$^{-1}$)

$\alpha_f$    surface heat transfer coefficient (W m$^{-2}$ K$^{-1}$)

$\alpha_{f\_corr}$    corrected surface heat transfer coefficient (W m$^{-2}$ K$^{-1}$)

$\lambda_f$    thermal conductivity (W m$^{-1}$ K$^{-1}$)

$\mu$    dynamic viscosity (Pa s)

$\mu_b$    bulk viscosity (Pa s)

$\mu_w$      wall viscosity (Pa s)

$\nu$      dynamic viscosity (m$^2$ s$^{-1}$)

$\rho$      density of agitated fluid (kg m$^{-3}$)

## Turbulence modeling nomenclature

$u_i$      instantaneous velocity

$\bar{u}_i$      mean velocity

$u'_i$      fluctuating velocity

$\overline{u'_i u'_j}$      Reynolds stresses

$\alpha^*$      damping coefficient causing a low Reynolds number correction

$k$      turbulent kinetic energy

$\varepsilon$      rate of dissipation of turbulence

$\omega$      specific dissipation rate

$\mu_t$      turbulent or Eddy viscosity

$\Phi$      scalar quantities

# Chapter 1.

# Introduction

Mixing operations are applied in a wide range of industries such as: petrochemicals, pharmaceuticals, polymer processing, biotechnology, food, industrial products, drinking water, wastewater treatment and many others. In all these industries, mixing operations are critical to obtain the required product. Moreover, problems in this stage could origin that the cost of manufacturing of the product increases significantly and subsequent losses because of delays.

"Although there are many industrial operations in which mixing requirements are readily scaled-up from established correlations, many operations require more detailed evaluation of the parameters involved". (Paul et al., 2004). To illustrate, one critical aspect during mixing operations is heat transfer. Depending on the application, it is frequently necessary to keep the temperature in some range to produce the required product yield or avoid undesired effects. When mixing operation requires heating or cooling, the vessel is equipped with additional devices such as jackets, coiled tubes or tube baffles to serve as an external heat source (sink). Furthermore, there are many geometry configurations that involve various parameters, which need to be considered to have good knowledge for designing of real equipment.

Heat transfer in stirred vessels has been researched extensively and many correlations have been published for different configurations. However, due to the diversity of parameters that are involved in specific geometries, there are different fields that still need to be studied in detail. Correlations for heat transfer are mainly based on experiments performed on scaled equipment, which can be applied to predict the heat transfer in real apparatuses for different industries. These experimental approaches need higher investment and time to obtain the required results. Nevertheless, taking advantage of the technological development, numerical simulation of fluid motion allows to simplify the process and obtain preliminary results with different conditions to get a better understanding of the phenomena. Finally, this information can be compared with verified correlations or experimental data to scale-up equipment for industrial applications.

The main objective of current study is to perform computational fluid dynamics (CFD) analysis of heat transfer in agitated vessel with a draft tube to obtain a correlation for heat transfer at the bottom. Based on some research that implies that there is similarity in the working principle with impinging jets, which is a widely studied topic.

# Chapter 2.

# Mixing technologies

There are different ways to perform mixing operations such as mechanical agitation, jets, gas sparging, and blending in-line in pipes, being mechanical mixing the most extensively applied method in different industries. Fluid mixing is carried out in mechanically stirred vessels for a variety of objectives, including for homogenizing single or multiple phases in terms of concentration of components, physical properties, and temperature. Some of the applications are blending of homogeneous liquids, suspending solids in crystallizers, blending and emulsification of liquids, dispersing gas in liquid, homogenizing viscous complex liquids and transferring heat through an external or internal device. (Paul et al., 2004)

## 2.1. Mechanical mixers

Figure 2.1 illustrates the standard parts of a conventional stirred tank; however, the correct geometry usually depends on the specific application. A brief explanation of some parts is following described:
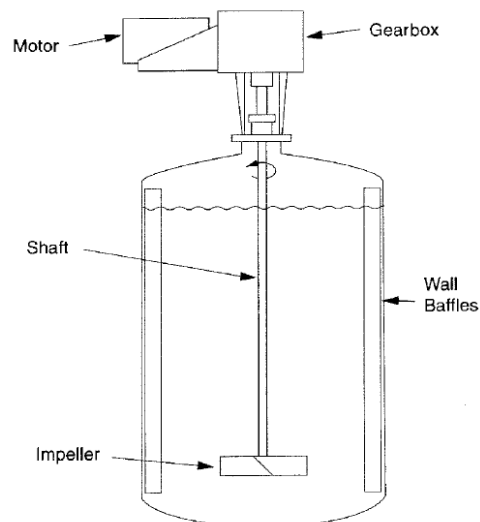
**Figure 2.1** *Conventional stirred tank*
Source: (Paul et al., 2004)

- Vessels: vertical cylinders, rectangular and horizontal.

- Impellers: devices that transmit rotational movement to the fluid allowing mixing. They can be classified according Table 2.1

**Table 2.1 Impeller Types** (Paul et al., 2004)

| Impeller | Specific types |
|---|---|
| Axial flow | Propeller, pitched blade turbine, hydrofoils |
| Radial flow | Flat-blade impeller, disk turbine (Rushton), hollow-blade turbine |
| High shear | Cowles, disk, bar, pointed blade impeller |
| Specialty | Retreat curve impeller, sweptback impeller, spring impeller, glass-lined turbines |
| Up/down | Disks, plate, circles |

- Heat transfer devices: when the process requires heating or cooling, the mixer is equipped by heat exchanger such as jacket, baffled jacket, baffle coil and helical coil.

- Wall baffles: solid bodies positioned in the path of tangential flows generated by the motion of the impeller. They transform tangential to vertical flows and help to avoid vortex effects and influence on the resulting mixing quality, but they increase the drag and the power draw of the impeller.

- Draft tube: is installed concentrically to the impeller axis with a diameter slightly larger than the impeller diameter. The effect of the axial flow generated by the impellers provides an efficient top-bottom circulation pattern.

The geometry subject to research is an agitated vessel with an axial 6-blade impeller (pitched angle 45º) placed in a draft tube with baffles in the upper part. As it was described before, an efficient top-bottom circulation is provided by the pumping channel (draft tube and flow generated by the impellers). In addition, the 45 pitched blade impeller generates axial flow that is commonly "used for blending, solids suspension, solids incorporation or draw down, gas inducement, and heat transfer." (Paul et al., 2004). Figure 2.2 shows a standard configuration of the stirred tank with a draft tube.
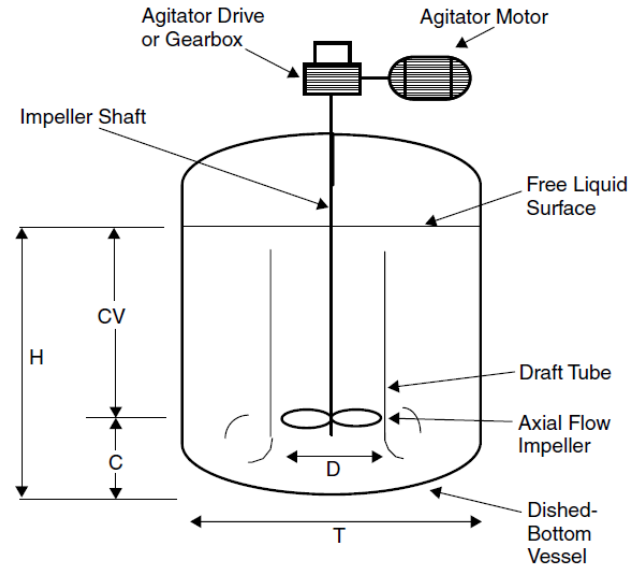
**Figure 2.2** *Stirred tank with a draft tube*
*Source: (Paul et al., 2004)*

## 2.2.  Impinging jets

Impinging jets can be used in a high shear mixing device to accomplish dispersion and mixing. These mixers usually operate as static devices, where the mixing power is provided by external high-pressure pump. There are several applications were impinging jets are used. For example, in the in-line mixers, they allow to reach high degrees of micromixing, so the blending of reagents should be completed to the molecular level in the minimum time. (Paul et al., 2004)

Other important applications are cooling, heating and drying, where "impinging jets are well established techniques for achieving high local convective heat transfer rates compared to other single-phase flow configurations." (Persoons et al., 2011) The working principle is a stream of fluid leaving a jet, which generally impacts a surface in normal direction, generating localized high heat transfer intensities. More information related to heat transfer and impinging jets is explained in the next chapter.

# Chapter 3.    Heat Transfer in agitated vessels

Heat transfer in agitated vessels has been researched extensively over the years. Many correlations have been published based on experimental work using different methods. Moreover, the magnitude of required heat transfer is obtained by heat and mass balances where a heat transfer coefficient has to be determined. This value is function of fluid properties and dimensionless groups.

The heat transfer rate in an agitated vessel depends on many parameters such as fluid properties, mixing intensity, geometry configuration, etc. Therefore, the influence of most of these parameters can be represented by heat transfer coefficient α which is shown in Eq. (1).

$$\dot{Q} = \alpha\ S\ \Delta T \tag{1}$$

Where:

$\dot{Q}$     hear transfer rate (W)

$\alpha$     heat transfer coefficient (W m$^{-2}$ K$^{-1}$)

$S$     heat transfer area (m$^2$)

$\Delta T$     temperature difference (K)

An energy balance in the vessel can be performed in order to get a relation of the heat transfer coefficient, and assuming that no reaction and no heat losses are present, the balance can be expressed as:

$$\dot{Q} = \alpha\ S\ (T_w - T) = m\ Cp\ \frac{dT}{dt} \tag{2}$$

Integrating the previous equation, the heat transfer coefficient can be evaluated by the following expression:

$$\alpha = \frac{m\ Cp}{S\ \Delta t} \ln\left(\frac{T_w - T_o}{T_w - T_f}\right) \tag{3}$$

Where:

$\alpha$      heat transfer coefficient ($W\,m^{-2}\,K^{-1}$)

$m$      mass (kg)

$c_p$      specific heat ($J\,kg^{-1}\,K^{-1}$)

$S$      heat transfer area ($m^2$)

$\Delta t$      time interval (s)

$T$      temperature of agitated liquid (K)

$T_w$      wall temperature (K)

$T_o$      initial temperature of agitated liquid (K)

$T_f$      final temperature of agitated liquid (K)

## 3.1. Dimensionless numbers

Heat transfer coefficient and operational parameters can be related by dimensionless numbers, which are described by the following equations:

### 3.1.1. Reynolds Number

In general, Reynolds number is the ratio between inertial forces over viscous forces. For a mixing system, the Reynolds number is expressed as follows:

$$\mathrm{Re_m} = \frac{n\,d_m{}^2\rho}{\mu} \tag{4}$$

Where:

$\mathrm{Re_m}$      Reynolds Number for a mixing system (-)

$n$      rotational speed of impeller ($s^{-1}$)

$d_m$      diameter of impeller (m)

$\rho$      density of agitated fluid ($kg\,m^{-3}$)

7

µ        dynamic viscosity (Pa s)

The Reynolds number can be used to determine the flow regime of the mixture, which allows to obtain the power consumed by a mixer or the heat transfer coefficient. Figure 3.1 illustrates the dependence of Re and power number (Np) for different kinds of impellers:
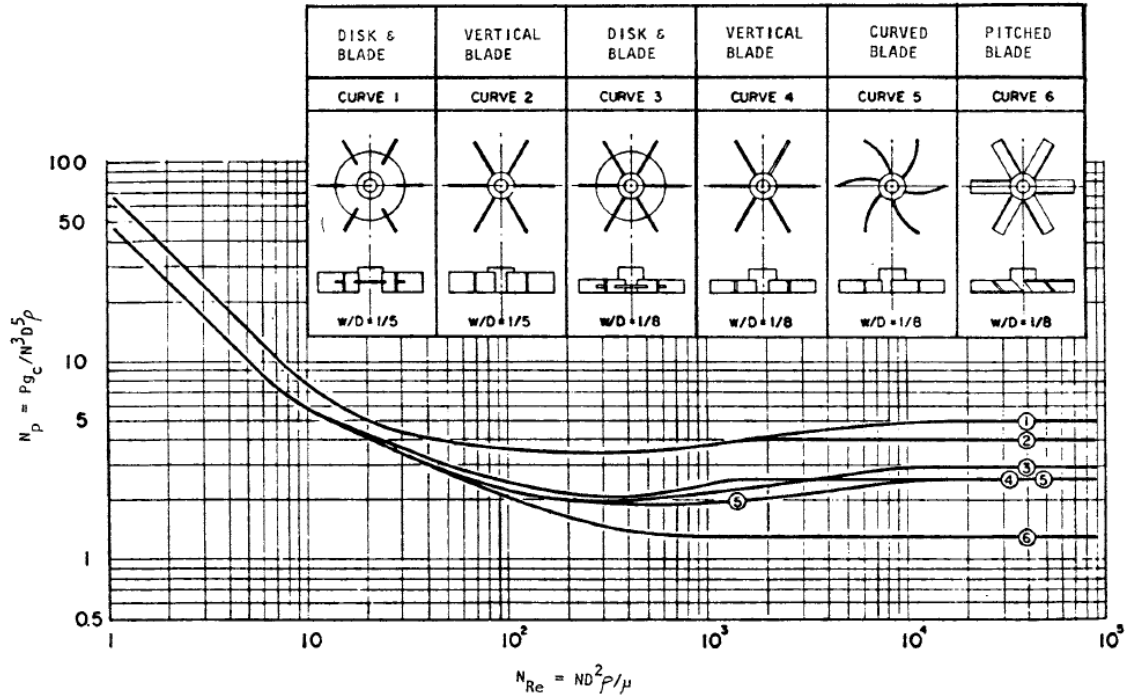


**Figure 3.1** *Power Number vs Reynolds*
*Source: (Couper et al., 2005)*

The dimensionless Reynolds number indicates the mixing flow regimes as follows:

- Laminar: below a Reynolds number of 10

- Transition between Reynolds numbers of 10 and $10^4$

- Turbulent above a Reynolds number of $10^4$

In addition, Reynolds Number for a jet was derived by (Petera et al., 2017) from Reynolds Number for a mixing system as follows:

$$\text{Re}_\text{m} = \text{Re} \frac{\pi\, d}{4\, d_m\, \text{N}_\text{Q}} \tag{5}$$

8

Where:

$Re_m$     Reynolds Number for a mixing system (-)

$Re$     Reynolds Number for a jet (-)

$d_m$     diameter of impeller (m)

$d$     inner diameter of the draft tube (m)

$N_Q$     dimensionless pumping capacity (-)

Eq. (5) considers a dimensionless number called pumping capacity $N_Q$, which depends on the geometry of the vessel considering its inner accessories. For this specific geometry, (Jirout et al., 2015) performed simulations and obtained pumping capacities shown in Table 3.1

**Table 3.1 Dimensionless numbers for several geometrical parameters on the impeller and draft tube** (Jirout et al., 2015)

| Pitched angle | $h/d$ | $N_Q$ | $W^*$ | $r^*$ |
|---|---|---|---|---|
| 30° | 1.0 | 0.381 | 0.1379 | 0.89 |
| | 0.5 | 0.368 | 0.1315 | 0.86 |
| | 0.25 | 0.332 | 0.1389 | 0.91 |
| 45° | 1.0 | 0.449 | 0.1817 | 0.89 |
| | 0.5 | 0.423 | 0.1786 | 0.92 |
| | 0.25 | 0.369 | 0.1789 | 0.91 |
| 60° | 1.0 | 0.437 | 0.2099 | 0.89 |
| | 0.5 | 0.410 | 0.2015 | 0.89 |
| | 0.25 | 0.356 | 0.2180 | 0.89 |

## 3.1.2. Prandtl Number

It is defined as the ratio of molecular diffusion of momentum over molecular diffusion of heat, and it depends on fluid properties that can be found in tables.

$$\mathrm{Pr} = \frac{\nu}{a} = \frac{\mu\, c_p}{\lambda_f} \tag{6}$$

Where:

Pr    Prandtl Number (-)

$\nu$    dynamic viscosity ($m^2\ s^{-1}$)

$a$    thermal diffusivity ($m^2\ s^{-1}$)

$c_p$    specific heat ($J\ kg^{-1}\ K^{-1}$)

$\lambda_f$    thermal conductivity ($W\ m^{-1}\ K^{-1}$)

### 3.1.3. Nusselt Number

It is the ratio between heat convection over heat conduction and is expressed as follows:

$$\text{Nu} = \frac{\alpha\ d}{\lambda_f} \tag{7}$$

Where:

Nu    Nusselt Number (-)

$\alpha$    heat transfer coefficient ($W\ m^{-2}\ K^{-1}$)

$d$    characteristic length, inner diameter of the draft tube (m)

$\lambda_f$    thermal conductivity ($W\ m^{-1}\ K^{-1}$)

For heat transfer, Nusselt number is general expressed as a relation between described dimensionless numbers:

$$\text{Nu} = C\ \text{Re}^p\ \text{Pr}^q\ \text{Vi}^s\ G_c \tag{8}$$

Where:

$$\text{Vi} = \frac{\mu_b}{\mu_w} \tag{9}$$

Nu    Nusselt Number (-)

$C$      precorrelation factor for Nu

Vi      Sieder-Tate factor for temperature dependency

$\mu_b$      bulk viscosity (Pa s)

$\mu_w$      wall viscosity (Pa s)

$G_c$      geometry correction factor

$p,q,s$   general exponents for dimensionless numbers

## 3.2. Heat transfer correlations

Due to similarities of working principle, some research has been done to compare impinging jets, which is a widely studied topic, with the axial flow generated by the impellers inside the draft tube. In both cases the discharging of fluid impacts over the bottom in normal direction, but they differ mainly in the tangential velocity component generated by the rotating impeller. Also, most of the information available for impinging jets is mainly for a smooth plane surface without being confined by the vessel walls. (Petera et al., 2017)

Previous research about heat transfer in an impinging jet was summarized by (Persoons et al., 2011), which shows different Nusselt number correlations. Table 3.2 illustrates an overview for steady jets.

**Table 3.2** Stagnation Nusselt number correlation for a steady jet *(Persoons et al., 2011)*

| Source | Jet type | $H/D$ | $Re$ | $Nu_0$ correlation in normalized form (Eq. (3)) |
|---|---|---|---|---|
| Shadlesky[3] | (a) Uniform jet[R, UC] | | | $0.5856Re^{1/2}Pr^{0.4}$ |
| | (b) Uniform jet[2D, UC] | | | $0.5051Re^{1/2}Pr^{0.4}$ |
| Liu and Sullivan [5] | Contoured nozzle[R, UC, Q] | 1–2 | 12,270–15,100 | $0.585Re^{1/2}Pr^{0.4}$ |
| Lytle and Webb [6] | (a) Uniform jet[R, UC] | <1 | | $0.540Re^{1/2}Pr^{0.4}(H/D)^{-1/2}$ |
| | (b) Long pipenozzle[R, UC, Q] | 0.25–1 | 3600–27,600 | $0.835Re^{0.53}Pr^{0.4}(H/D)^{-0.19}$ |
| Kataokaet al. [7] | Contoured nozzle[R, C, T] | 2–10 | 7000–50,000 | $(0.82 + fn(TuRe^{1/2}))Re^{1/2}Pr^{1/2}$ |
| Garimella and Rice [9] | Sharp orifice[R, C, Q] | 1–5 | 4000–23,000 | $0.462Re^{0.585}Pr^{0.4}(H/D)^{0.024}$ |
| | | 6–14 | 4000–23,000 | $0.499Re^{0.694}Pr^{0.4}(H/D)^{-0.56}$ |
| Zumbrunnen and Aziz [11] | Contoured nozzle[2D, UC, Q] | 7 | 3100–20,750 | $0.230Re^{0.589}Pr^{0.4}$ |

R = axisymmetric, 2D = two-dimensional, (U)C = (un)confined, T = isothermal heating, Q = constant heat flux.

For this study, the correlations following described will be used to compare the heat transfer coefficient at the bottom obtained by CFD.

First, a correlation for the heat transfer coefficient at bottom obtained by (Petera, 2017) will be applied. This correlation is described by Eq. (10) and was the result of performing simulations in ANSYS Fluent, based on Moving Reference Frame approach.

$$\overline{\mathrm{Nu}} = 0{,}101 \, \mathrm{Re_m}^{0{,}680} \mathrm{Pr}^{1/3} \tag{10}$$

Then, a correlation describing the Nusselt number for the agitated vessel with a draft tube, published by (Petera et al., 2017) will be used for the same purpose. This correlation was obtained by measuring the local values of heat transfer coefficients at the vessel bottom by the electrodiffusion method. In addition, it is important to mention that this equation does not consider the Sieder-Tate factor for temperature dependency Eq. (9), which is normally solved by an iterative process, but can result in more accurate results.

$$\overline{\mathrm{Nu}} = 0{,}041 \, \mathrm{Re}^{0{,}826} \, \mathrm{Pr}^{1/3} \left(\frac{h}{d}\right)^{-0{,}099} \mathrm{Sw}^{0{,}609} \tag{11}$$

Where:

$\overline{\mathrm{Nu}}$     Mean Nusselt Number (-)

Re     Reynolds Number for a jet (-)

Pr     Prandtl Number (-)

$h$     distance of draft tube from bottom (m)

$d$     inner diameter of the draft tube (m)

Sw     Swirl number (-)

According to research published on the article Heat Transfer at the bottom of a cylindrical vessel impinged by a swirling flow from an impeller in a draft tube, "the tangential velocity component superposed on the main axial velocity component has a significant impact on the heat transfer intensity in an impinging jet. Some authors describe the influence of the tangential velocity component by the Swirl number" (Petera et al., 2017).

$$Sw = \frac{8\,W}{15\,U} \tag{12}$$

Where:

*W*      tangential velocity (m s$^{-1}$)

*U*      mean velocity in the axial direction (m s$^{-1}$)

For the case of the study geometry, the relation *W/U* for Eq. (12) can be expressed as follows (Petera et al., 2017) and be evaluated using values from Table 3.1:

$$\frac{W}{U} = \frac{\pi^2}{4}\left(\frac{d}{d_m}\right)^2 \frac{W^*}{N_Q} \tag{13}$$

Where:

$W^*$      Dimensionless maximum tangential velocity at the outlet of the draft tube

$N_Q$      dimensionless pumping capacity (-)

For the correlation shown in Eq. (11), the valid range of dimensionless distance is 0,25 ≤ *h/d* ≤ 1. The confidence intervals of individual parameters determined in the non-linear least-squares regression analysis are as follows:

$$0,041 \pm 0,005;\ 0,826 \pm 0,013;\ -0,099 \pm 0,010;\ 0,609 \pm 0,036$$

# Chapter 4.  Computational Fluid Dynamics

Computational fluid dynamics (CFD), the numerical simulation of fluid motion, has advanced significantly in the last years and has become an important tool for researching, industrial process design, troubleshooting, and retrofit. Currently, one application where CFD is extensively used is industrial mixing because it helps to understand the flow and mixing qualitatively and quantitatively. (Kresta et al., 2016)

Modeling a stirred tank using CFD requires consideration of many aspects of the process. First, any computational model requires that the domain of interest, in this case the volume occupied by the fluid inside the vessel, be described by a computational grid, a set of cells. It is in these cells that problem-specific variables are computed and stored. The computational mesh must fit the contours of the vessel and its internals, even if the components are geometrically complex. Second, the motion of the impeller in the tank must be treated in a special way, especially if the tank contains baffles, draft tubes or other internals. The special treatment employed affects both the construction of the computational grid and the solution method used to obtain the flow field numerically. (Paul et al., 2004)

## 4.1.  Fundamental equations

The solution of CFD is based on the numerical solution of conservation equations that govern fluid motion. This approach discretizes the Navier-Stokes equations into a system of algebraic equations to provide quantitative predictions. The following principles describe typical phenomena for mixing operations with heat transfer.

### 4.1.1. Continuity

The continuity equation represents a conservation of molar and mass fluxes of some system. For the current case where water is the fluid can be expressed as:

$$\frac{\partial \rho}{\partial t} + \nabla . (\vec{u} \, \rho) = 0 \qquad (14)$$

Where:

| | |
|---|---|
| $\rho$ | Density |
| $\frac{\partial \rho}{\partial t}$ | Rate of element accumulation |
| $\nabla.\left(\vec{u}\rho\right)$ | Convective income of element |

For incompressible fluids Eq (14) transforms to:

$$\nabla.\vec{u} = 0 \tag{15}$$

## 4.1.2. Momentum

The momentum equation represents conservation of momentum in each of the three component directions. This equation, called Navier Stokes equation, is a special case of Cauchy's equation.

$$\rho\left(\frac{\partial \vec{u}}{\partial t} + \vec{u}.\nabla\vec{u}\right) = -\nabla p + \mu\nabla^2\vec{u} + \rho\vec{g} \tag{16}$$

Where:

$\nabla p$      Gradient of pressure

$\mu\nabla^2\vec{u}$      Tensor of viscous forces

$\rho\vec{g}$      Gravity force

## 4.1.3. Energy

The principle for conservation of energy is the fundamental equation to calculate heat transfer:

$$\rho\frac{D}{Dt}\left(U + \frac{\vec{u}^2}{2} + \varphi\right) = -\nabla.\vec{q} + \vec{\vec{\tau}}:\vec{\vec{\Delta}} + \dot{Q}^{(g)} \tag{17}$$

Where:

The left sight of the equation represents material derivative of total energy (internal, kinetic and potential energy respectively).

$\nabla . \vec{q}$      Convective heat flux

$\vec{\tau} : \vec{\Delta}$      Dissipation of mechanical energy to heat

$\dot{Q}^{(g)}$      Internal source of heat

After some manipulation and simplifications, Eq. (17) will transform to the Fourier-Kirchoff equation, Eq. (18). The solution of the Fourier-Kirchoff equation results in the temperature distribution (field) in some system (Petera, 2017).

$$\rho \, C_p \left( \frac{\partial T}{\partial t} + \vec{u} . \nabla T \right) = -\nabla . \vec{q} + \vec{\tau} : \vec{\Delta} + \dot{Q}^{(g)} \tag{18}$$

## 4.2. Turbulence models

Based on values of the Reynold numbers, flow regime can be defined as laminar or turbulent as it was described in the previous chapter. In general, turbulent regime cannot be solved analytically. Therefore, numerical methods allow to obtain an approximation of the solution by discretizing the Navier-Stokes equations into algebraic equations. "The discrete equations are derived using finite differences or finite volumes, linking the different grid points together" (Kundu et al., 2016). However, to obtain meaningful results, different aspects must be considered into the CFD model. Three basic approaches can be used to calculate a turbulent flow:

- Direct Numerical Simulation (DNS)

- Large Eddy Simulation (LES)

- Reynolds Averaged Navier Stokes Simulation (RANS)

The current study was performed in ANSYS Fluent, and RANS based models were applied. These approaches are the most widely used for industrial flows. (ANSYS 15.0 Training Materials, 2013)

## 4.2.1. Reynolds Averaged Navier Stokes Simulation (RANS)

These methods involve a process of time averaging the conservation equations, where the solution variables in the instantaneous equations are decomposed into mean and fluctuating components. For the velocity components:

$$u_i = \bar{u}_i + u'_i \tag{19}$$

Where:

$u_i$      instantaneous velocity

$\bar{u}_i$      mean velocity

$u'_i$      fluctuating velocity

Similarly, for pressure and other scalar quantities:

$$\phi = \bar{\phi} + \phi' \tag{20}$$

Where Φ denotes scalar quantities such as pressure or concentration

Substituting these expressions into the instantaneous conservations equations, RANS equations are obtained as follows:

$$\frac{\partial \rho}{\partial t} + \frac{\partial}{\partial x_i}(\rho \bar{u}_i) = 0 \tag{21}$$

$$\frac{\partial(\rho \bar{u}_i)}{\partial t} + \frac{\partial(\rho \bar{u}_i \bar{u}_j)}{\partial x_j} = -\frac{\partial \bar{p}}{\partial x_i} + \frac{\partial}{\partial x_j}\left[\mu\left(\frac{\partial \bar{u}_i}{\partial x_j} + \frac{\partial \bar{u}_j}{\partial x_i} - \frac{2}{3}\delta_{ij}\frac{\partial \bar{u}_k}{\partial x_k}\right)\right] + \frac{\partial}{\partial x_j}(-\rho \overline{u'_i u'_j}) \tag{22}$$

Where:

$\overline{u'_i u'_j}$    Reynolds stresses

Additional terms, called Reynolds stresses, represent the effects of turbulence and need to be related to other variables. This is done through various models, known as turbulence models.

Applying the assumption of Boussinesq hypothesis, Reynolds stresses can be expressed in terms of mean velocity gradients. (Paul et al., 2004)

$$\rho\overline{u'_i u'_j} = \frac{2}{3}\rho k\delta_{ij} + \left[\mu_t\left(\frac{\partial\overline{u_i}}{\partial x_j} + \frac{\partial\overline{u_j}}{\partial x_i}\right)\right] \tag{23}$$

Where:

$k$       Turbulent kinetic energy

$\mu_t$       Turbulent or Eddy viscosity

## 4.2.2. RANS based turbulence models

The RANS turbulence models allow to compute the Reynolds stresses for substitution into Eq. (22) and apply approximations to calculate unknown parameters. The list of RANS based models available in Fluent are shown below, in which the computational demand increases with the number of equations

- One-Equation Model      Spalart-Allmaras

- Two-Equation Models      Standard k–ε

                                          RNG k–ε

                                          Realizable k–ε

                                          Standard k–ω

                                          SST k–ω

- Three-Equation Model      k–kl–ω Transition Model

- Four-Equation Model      SST Transition Model

- Seven-Equation Model      Reynolds Stress Model

Two-equation model was used for the current study where 2 transport equations are solved, giving two independent scales for calculating turbulent viscosity:

$$\rho \frac{Dk}{Dt} = \frac{\partial}{\partial x_j}\left[\left(\mu + \frac{\mu_t}{\sigma_k}\right)\frac{\partial k}{\partial x_j}\right] + P - \rho\varepsilon \tag{24}$$

$$P = \mu_t S^2 \tag{25}$$

$$S = \sqrt{2S_{ij}S_{ij}} \tag{26}$$

$$S_{ij} = \frac{1}{2}\left(\frac{\partial U_i}{\partial x_j} + \frac{\partial U_j}{\partial x_i}\right) \tag{27}$$

Where:

k        Turbulent kinetic energy

ε        Rate of dissipation of turbulence

$\mu_t$        Turbulent viscosity

P        Generation term for turbulence

$\sigma_k$        Empirical constant

### k-ε Model

This semiempirical method is a robust and reasonably accurate model for a wide range of applications and is applicable to an extensive variety of turbulent flows, being most widely used engineering turbulence model for industrial applications. (ANSYS 15.0 Training Materials, 2013) To compute Reynolds stresses, two additional transport equations must be solved:

$$\mu_t = \rho C_\mu \frac{k^2}{\varepsilon} \tag{28}$$

Where:

k        Turbulent kinetic energy

ε        Rate of dissipation of turbulence

$\mu_t$        Turbulent viscosity

$C_\mu$        Empirical constant

**k - Transport equation**

$$\rho \frac{Dk}{Dt} = \frac{\partial}{\partial x_j}\left[\left(\mu + \frac{\mu_t}{\sigma_k}\right)\frac{\partial k}{\partial x_j}\right] + \mu_t S^2 - \rho\varepsilon \tag{29}$$

**ε - Transport equation**

$$\rho \frac{D\varepsilon}{Dt} = \frac{\partial}{\partial x_j}\left[\left(\mu + \frac{\mu_t}{\sigma_k}\right)\frac{\partial \varepsilon}{\partial x_j}\right] + \frac{\varepsilon}{k}(C_{1\varepsilon}\mu_t S^2 - \rho C_{2\varepsilon}\varepsilon) \tag{30}$$

### *k-ω Model*

It is an empirical model based on transport equations for the turbulence kinetic energy (k) and the specific dissipation rate (ω), which can be expressed as follows:

$$\omega \approx \frac{\varepsilon}{k} \tag{31}$$

This model is accurate and robust for a wide range of boundary layer flows with pressure gradient, and its performance is much better than k- ε models for boundary layer flows, but one of the weak aspects is the sensitivity of the solutions to values for k and ω outside the shear layer. (ANSYS, INC, 2013)

$$\mu_t = \alpha^* \rho \frac{k}{\omega} \tag{32}$$

Where:

$\alpha^*$        Damping coefficient causing a low Reynolds number correction

**k - Transport equation**

$$\rho \frac{Dk}{Dt} = \frac{\partial}{\partial x_j}\left[\left(\mu + \frac{\mu_t}{\sigma_k}\right)\frac{\partial k}{\partial x_j}\right] + \tau_{ij}\frac{\partial \bar{u}_i}{\partial x_j} - \rho\beta^* f_{\beta^*} k\omega \tag{33}$$

**ω - Transport equation**

$$\rho \frac{D\omega}{Dt} = \frac{\partial}{\partial x_j}\left[\left(\mu + \frac{\mu_t}{\sigma_\omega}\right)\frac{\partial \omega}{\partial x_j}\right] + \alpha\frac{\omega}{k}\tau_{ij}\frac{\partial \bar{u}_i}{\partial x_j} - \rho\beta f_\beta \omega^2 \tag{34}$$

### *Shear Stress Transport (SST) k-ω Model*

The SST model is a hybrid two-equation model that combines the advantages of both k-ε and k-ω models. "This model blends the robust and accurate formulation of the k-ω model in the near-wall region with the freestream independence of the k-ε model in the far field. The SST k-ω is similar to the standard k-ω model, but it includes some refinements as the definition of the turbulent viscosity that is modified to account for the transport of the turbulent shear stress." (ANSYS, INC, 2013).

$$\mu_t = \rho \frac{k}{\omega} \frac{1}{max\left[\frac{1}{\alpha^*}, \frac{SF_2}{a_1\omega}\right]} \tag{35}$$

Where:

$S$        Strain rate magnitude

$F_2$        Blending function

Due to its advantages, SST k-ω model is a recommended choice for mixing applications. Therefore, the set of simulations for the current study were performed by applying this model and additional options were activated as Production Limiter, Production Kato-Lauder and Intermittency Transition Model that will be mentioned in the next chapters.

# Chapter 5.  Geometry and Mesh description

The geometry and mesh used for this study were the same than the applied for a previous thesis entitled CFD simulation of heat transfer in an agitated vessel with a draft tube (Calvopina, 2018). As it was mentioned in previous chapters, the agitated vessel contains an impeller with 6 blades (pitched angle 45º) placed in a draft tube with baffles in the upper part, where the relation of the draft tube to the bottom ($h/d$) was changed to 1, 0,5 and 0,25, to evaluate that effect in the heat transfer. "Such small distances (0.25 ≤ $h/d$ ≤ 1) are typical for mixing of liquids, which ensures good homogenization and increases the intensity of heat and mass transfer in many industrial operations." (Petera et al., 2017) The geometry configuration and the main dimensions are shown in Figure 5.1.



H = 430 mm

D = 392 mm

h = 70 mm

d = 70 mm

dm = 61 mm
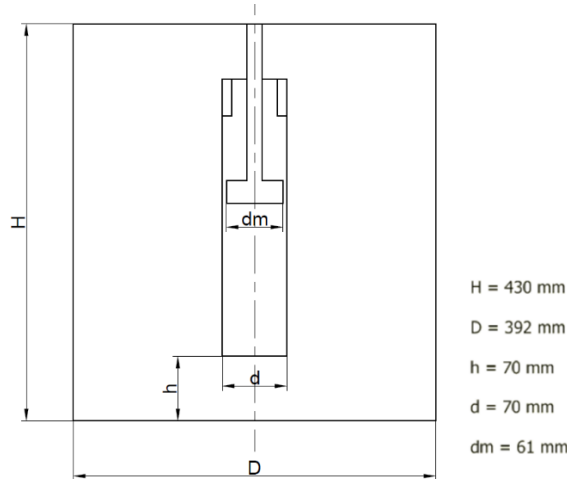
*Figure 5.1* Geometry configuration

## 5.1.  Geometry

The geometry shown in Figure 5.2, is composed of multiple bodies in order to use different meshing methods. There are two main parts: the impeller zone (light green body) and the surroundings, this last one is divided in 12 parts containing: zones above and below the impeller, zone inside the draft tube with baffles, zone outside the diffusor and 8 more zones representing the outer fluid.
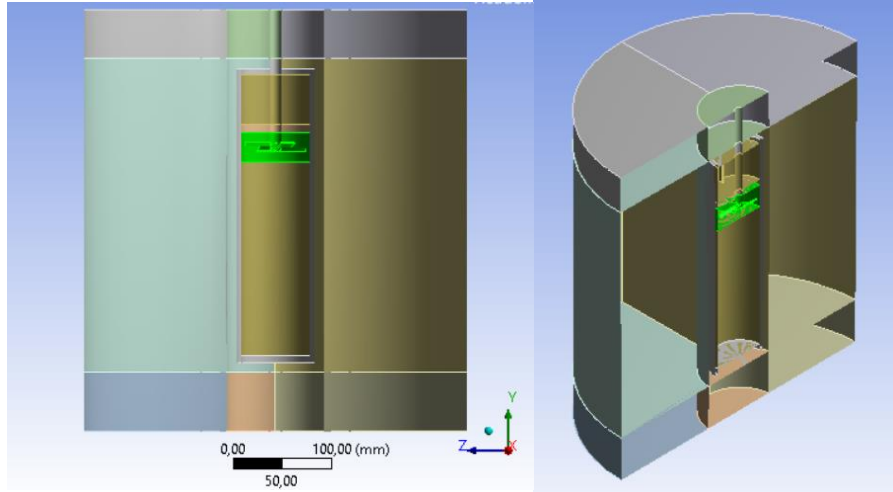
***Figure 5.2*** Geometry description

## 5.2. Mesh

The main meshing methods used are described according to the numbers shown in Figure 5.3,
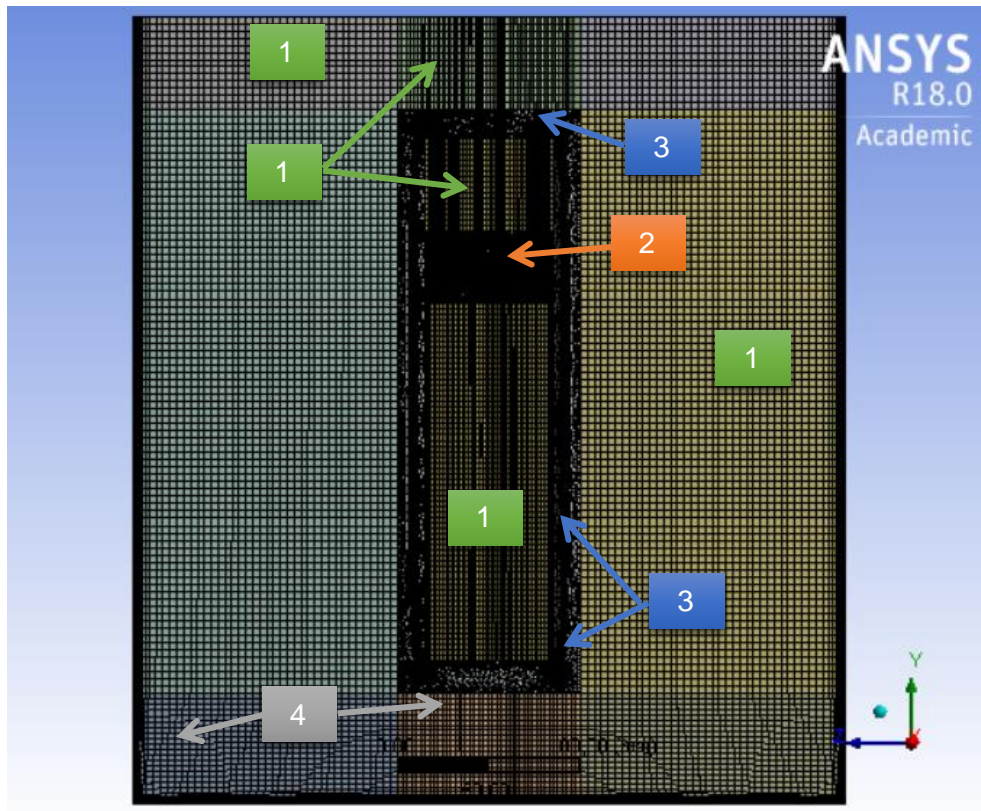


***Figure 5.3*** Meshing methods

**1.** Sweep method was used for the inner fluid (diffusor top and bottom) and outer fluid (upper and middle part), with element size 3mm and 4 mm respectively.

**2.** Tetrahedrons method with Patch conforming was set for the impeller zone, with element size 1,6 mm for the body and 0,5 mm for the blades, and curvature as size function.

**3.** For zone around the diffusor, Tetrahedrons method with Patch conforming was used, element size was set according to global settings.

**4.** For the bottom zone, multizone meshing was used with hexahedral elements, and 3mm as Sweep element size.

Inflation was applied to the impeller, inside and outside of the diffusor and bottom part to capture boundary layer gradients.

### 5.2.1. Mesh quality

The Global settings were established for Sizing as: Size function: Curvature, Transition: Slow, Span angle center: Fine, and for Quality: Smoothing: medium. The mesh metrics for this model are summarized in Table 5.1.

**Table 5.1 Mesh metrics**

| Mesh Metric | Value | Mesh quality recommendations (*) | Comments |
|---|---|---|---|
| Nodes | 1584665 | - | - |
| Elements | 2666580 | - | - |
| Min. Orthogonal Quality | 0,08054 | Min > 0,1 Values: (0-1) | $\approx$ 84% of elements > 0,75 |
| Max. Skewness | 0,92768 | Max < 0,95 | OK |
| Max. Aspect Ratio | 374,94 | < 10-100 | $\approx$ 3% of elements > 100 |

Note: * ANSYS. Mesh Quality & Advanced Topics

### 5.2.2. Grid Convergence Index

A previous analysis was performed by (Chakravarty, 2017) to determine the appropriate mesh size for unsteady heat transfer with reasonable accuracy in the agitated vessel. The study was evaluated with three different number of mesh elements: 1,1, 2,3

and 4,5 million. As a result, it was found that for the mesh with around 2 million mesh elements, the numerical uncertainty was 1,08%.

The number of mesh elements for the current case were over 2,5 million, so it could be predicted that the results will be satisfactory accurate.

# Chapter 6.    Numerical simulations

The simulations were performed in ANSYS Fluent, 18.2 research version, on Czech Technical University's servers, using the Moving Reference Frame (MRF) approach because lower computational requirements compared to Sliding Mesh Method. This Sliding Mesh method was used in a previous study (Calvopina, 2018), but the high computational demand restricted to perform several simulations for longer time ranges although the simulations were conducted using the university's servers. The MRF method allows the user to model the flow around the moving part (with certain restrictions) as a steady-state problem with respect to the moving frame. In this case, the fluid region containing the impeller zone was set as Moving Reference Frame with a constant rotational speed, and the fluid-outer zone remained static.

In Fluent, pressure based solver was chosen as the numerical method for the solution, in this approach "the velocity field is obtained from the momentum equations, and the pressure field is extracted by solving a pressure or pressure correction equation which is obtained by manipulating continuity and momentum equations". (ANSYS, INC, 2013)

The current project was performed according to the following sequence, and SST k-ω model was applied for all the simulations.

1. Comparison of heat transfer coefficient obtained by different methods and analysis of simulated time interval.

2. Comparison between SST k- ω vs SST k- ω with intermittency Transition Model activated.

3. Simulations for different position of the draft tube with respect to the vessel bottom.

4. Determination of Nusselt number correlation.

The following initial and boundary conditions were considered for the current study:

**Initial condition**, temperature of the fluid of 300K at t=0s.

**Boundary conditions**, temperature at the bottom wall of 400K and:

*For the first stage:* rotational speed of 600 rpm (around Y-axis) for intervals of (0-10), (10-30), (30-50), (50-100), (100-150), (150-200) seconds.

*For the rest of simulations:* range of speeds 300, 400, 500, 600, 700, 800, 900, 1000 and 1200 rpm.

Water was used as working fluid at 300 K. Table 6.1 shows the fluid and geometry properties. These values were retrieved from ANSYS-Fluent and set as constants for the simulations and the calculations.

**Table 6.1 Water properties at 300K and geometry**

| Property | Unit | Value |
|---|---|---|
| Cp | $(J.kg^{-1}.K^{-1})$ | 4182 |
| ρ | $(kg.m^{-3})$ | 998,2 |
| λ_f | $(W.m^{-1}.K^{-1})$ | 0,6 |
| μ | $(kg.m^{-1}.s^{-1})$ | 0,001003 |
| V | $(m^3)$ | 0,050974629 |
| S | $(m^2)$ | 0,11940941 |
| m(water) | (kg) | 50,882875 |

## 6.1. Comparison of heat transfer coefficient obtained by different methods and analysis of simulated time interval

During the first stage, a set of simulations from 0 to 200 seconds was performed using SST k-ω model with Production Limiter option activated "in order to avoid the buildup of turbulent kinetic energy in the vicinity of stagnation regions. This limiter is set by default for all turbulence models based on ω equation" (ANSYS, INC, 2013).

The time step selected was Δt=0,01s to reduce the time demand because several sets of simulations were performed during this study. Table 6.2 shows simulations settings for the different intervals.

**Table 6.2 Simulations settings**

| Intervals (s) | Time simulation (s) | Number of time steps | Max iteration/ timestep |
|---|---|---|---|
| 0-10 | 10 | 1000 | 20 |
| 10-30 | 20 | 2000 | 20 |
| 30-50 | 20 | 2000 | 20 |
| 50-100 | 50 | 5000 | 20 |

| Intervals (s) | Time simulation (s) | Number of time steps | Max iteration/ timestep |
|---|---|---|---|
| 100-150 | 50 | 5000 | 20 |
| 150-200 | 50 | 5000 | 20 |

Convergence criteria was set according to Figure 6.1 for every interval with standard initialization. Then, the simulations were run until the residuals were lower than the set values, resulting in all equations converged for every interval.
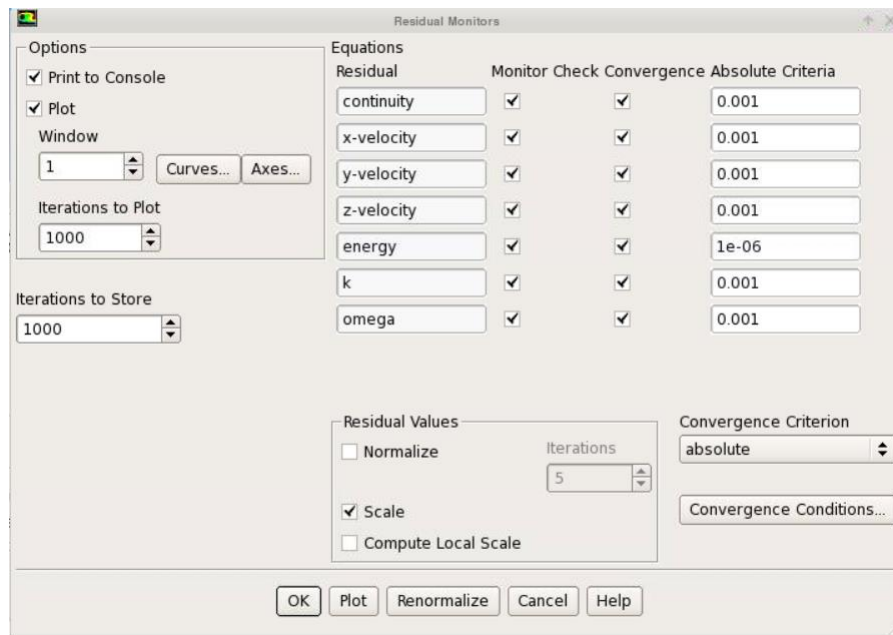


**Figure 6.1** Residuals criteria

Table 6.3 illustrates the results of the simulations obtained in ANSYS Fluent, where 3 values for heat transfer coefficient at the bottom were found. The first one is the value retrieved from Fluent directly. The second one is the value computed by using energy balance (Eq.3), which uses initial and final temperatures from the simulations and geometrical and fluid properties from Table 6.1. Finally, the heat transfer coefficient from Fluent with a correction factor was evaluated.

The reason that the last value needs to be adjusted is because the report in Fluent uses Eq.(36) to calculate the surface heat transfer coefficient, where $T_{ref}$ is the temperature of the liquid specified by the user. (ANSYS 15.0 Training Materials, 2013) Consequently, while the temperature of the liquid is kept as constant (not increasing with the time), the inaccuracy of the surface heat transfer coefficient will growth as time goes on.

$$\alpha_f = \frac{q_w}{T_w - T_{ref}} \tag{36}$$

Where:

$\alpha_f$    surface heat transfer coefficient (W m$^{-2}$ K$^{-1}$)

$q_w$    heat flux (W m$^{-2}$)

$T_w$    wall temperature (K)

$T_{ref}$    reference temperature of the liquid (K)

The correction factor was calculated according Chakravarty's proposal, who computed heat flux $q_w$ by Eq.(36) and recalculated the surface heat transfer coefficient considering Log Mean Temperature Difference (LMTD) instead of $T_w - T_{ref}$ (Chakravarty, 2017).

$$\alpha_{f\_corr} = \frac{q_w}{\overline{\Delta T}_{ln}} \tag{37}$$

$$\overline{\Delta T}_{ln} = \frac{(T_w - T_{ref}) - (T_w - T_b)}{\ln\left(\frac{T_w - T_{ref}}{T_w - T_b}\right)} \tag{38}$$

Where:

$\alpha_{f\_corr}$    corrected surface heat transfer coefficient (W m$^{-2}$ K$^{-1}$)

$T_b$    final temperature of the batch (K)

**Table 6.3 Results and calculation, 600 rpm**

| Interval (s) | 0-10 | 10-30 | 30-50 | 50-100 | 100-150 | 150-200 |
|---|---|---|---|---|---|---|
| $\Delta$t (s) | 10 | 20 | 20 | 50 | 50 | 50 |
| To (K) | 300,000 | 301,287 | 303,759 | 306,170 | 311,941 | 317,359 |
| *Tf (K) | 301,287 | 303,759 | 306,170 | 311,941 | 317,359 | 322,458 |
| Tw (K) | 400,000 | 400,000 | 400,000 | 400,000 | 400,000 | 400,000 |
| **$\alpha_f$ (W m$^{-2}$ K$^{-1}$) | 2294,261 | 2232,625 | 2199,060 | 2127,835 | 2062,175 | 2000,943 |
| $\alpha_{IM}$ (W m$^{-2}$ K$^{-1}$) | 2308,923 | 2259,038 | 2261,273 | 2262,306 | 2263,183 | 2269,880 |
| $\alpha_{f\_corr}$ (W m$^{-2}$ K$^{-1}$) | 2309,156 | 2275,664 | 2269,830 | 2265,993 | 2265,009 | 2266,190 |

Notes:    *Temperatures were retrieved from Fluent Solver by displaying: Reports, Volume Integrals, Report Type: Mass Average, Field Variable: Temperature- Total Temperature (inner and outer fluid).
** Heat transfer coefficients were retrieved from Fluent Solver by displaying: Surface Integrals, Report type: Area-Weighted Average, Field Variable: Unsteady Wall Statistics- Mean Surface Heat Transfer Coeff.

Plotting the results, Figure 6.2 shows how the surface heat transfer coefficient from fluent decreased while time went on, and by applying the correction factor, the heat transfer coefficient got closer to the one calculated by energy balance (Integral Method $\alpha_{\_IM}$). This method was used as reference for the subsequent results.



| | 10 | 30 | 50 | 100 | 150 | 200 |
|---|---|---|---|---|---|---|
| α-f | 2294,26 | 2232,62 | 2199,06 | 2127,84 | 2062,17 | 2000,94 |
| α_ IM | 2308,92 | 2259,04 | 2261,27 | 2262,31 | 2263,18 | 2269,88 |
| α_f_c | 2309,16 | 2275,66 | 2269,83 | 2265,99 | 2265,01 | 2266,19 |
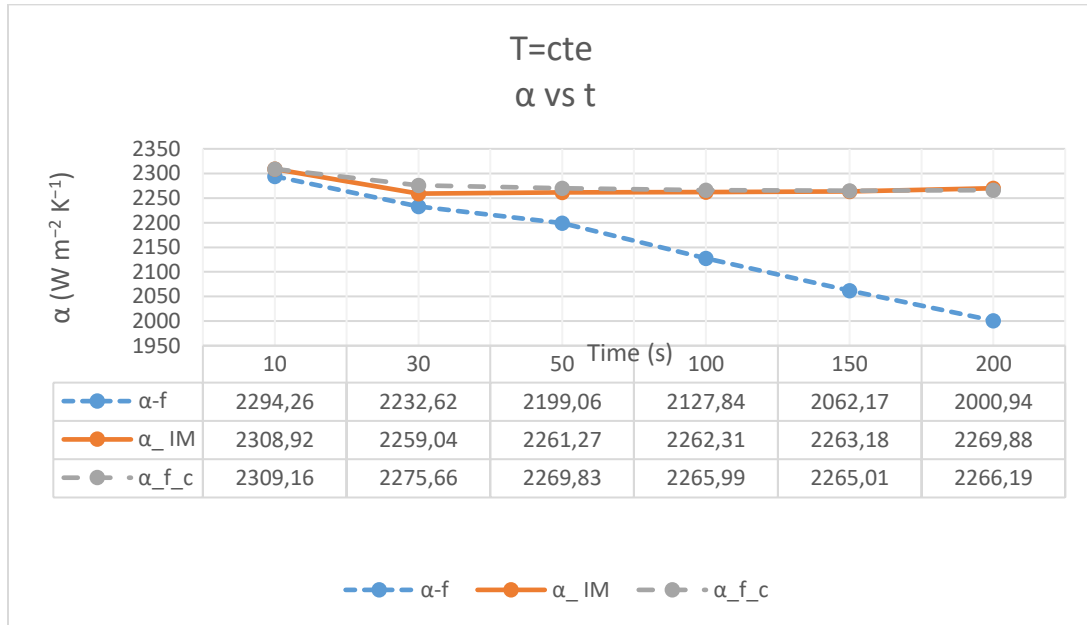
**Figure 6.2** Heat transfer coefficients comparison

In addition, it can be noticed that after 50 seconds, the heat transfer coefficient (HTC) had a very slight variation, so this time was chosen for the following set of simulations. The variation of heat transfer coefficient through time is shown in Table 6.4, which illustrates the absolute percentage difference by comparing the variation of the actual value with the previous one. $\left|\frac{\alpha_t - \alpha_{t+\Delta t}}{\alpha_t}\right|$

**Table 6.4 Time dependence of heat transfer coefficient for different methods.**

| t(s) | 10 | 30 | 50 | 100 | 150 | 200 |
|---|---|---|---|---|---|---|
| $\alpha_f$ (W m$^{-2}$ K$^{-1}$) | - | 2,69% | 1,50% | 3,24% | 3,09% | 2,97% |
| $\alpha_{IM}$ (W m$^{-2}$ K$^{-1}$) | - | 2,16% | 0,10% | 0,05% | 0,04% | 0,30% |
| $\alpha_{f\_corr}$ (W m$^{-2}$ K$^{-1}$) | - | 1,45% | 0,26% | 0,17% | 0,04% | 0,05% |

## 6.2. Comparison between SST k- ω vs SST k- ω with intermittency Transition Model activated

Two set of simulations with different activated options were performed in order to be compared. The initial and boundary conditions mentioned in the introduction of this chapter were established for the relation *h/d* = 1.

First, SST k-ω model was used with Production Limiter and Production Kato-Launder options activated. These production terms in the turbulence equations can limit the buildup of turbulent kinetic energy in stagnation points. "The formulation based on the work of Kato and Launder mentions that the excessive level of turbulence kinetic energy is caused by the very high level of shear strain rate in the stagnation regions". (ANSYS, INC, 2013). For this case, production terms are recommended because a stagnation point is present, and the overproduction of turbulent kinetic energy at that location will cause the model to yield inaccurate predictions at high Reynolds numbers. (Langel et al., 2016)

Then, SST k-ω was applied with intermittency Transition Model activated, which solves only one transport equation for the turbulence intermittence, avoiding the second equation of the Transition SST model. This model presents the advantages of reducing computational demand by solving one transport equation and avoiding the dependency of the Reynolds equation on the velocity (ANSYS, INC, 2013). In addition, Production Limiter and Production Kato-Launder were activated to avoid undesired effects as it was mention before.

The set of simulations were performed in two stages keeping the time step of $\Delta t=0,01s$. First, 2000 steady state iterations were run to obtain a fully developed flow profile in the system. Then, the energy model was switched to transient model, and simulations for 50 seconds (5000 iterations) were performed for the different rotational speeds.

The residual settings for the first set of simulations were kept the same as the previous case, while for the simulations with the intermittency Transition Model activated were set according to Figure 6.3. It can be noticed that the variations were: for continuity equation 1e-04, for energy 1e-07 and 1e-03 for an additional intermittency residual.
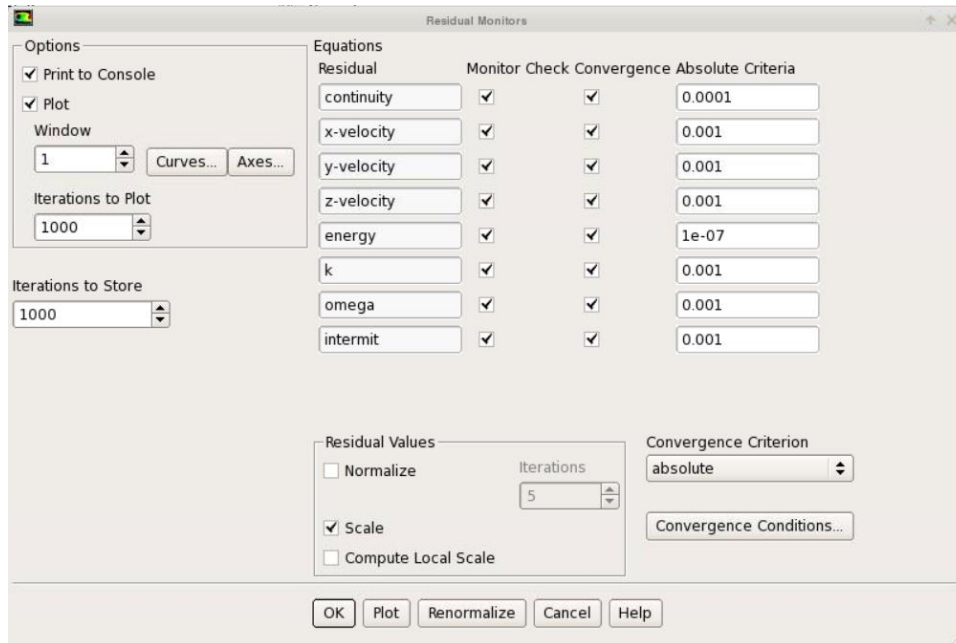
**Figure 6.3** Residuals criteria, Intermittency Transition Model

After the convergence was obtained, the results are summarized in Table 6.5 and Table 6.6. They show 3 values of heat transfer coefficient, using the same methodology that was described previously. Additionally, Reynolds number for a mixing system and Reynolds number for a jet were evaluated by using Eq. (4) and Eq. (5) respectively. The value for pumping capacity was retrieved from Table 3.1 for Eq. (5).

**Table 6.5 Results and calculations for simulations SST k-ω model with Production Limiter and Production Kato-Launder options activated, *h/d*=1**

| n (rpm) | $\Delta t$ (s) | Tb-o (K) | Tb-f (K) | Tw (K) | Re-m (-) | Re (-) | $\alpha_f$ (W m$^{-2}$K$^{-1}$) | $\alpha_{IM}$ (W m$^{-2}$K$^{-1}$) | $\alpha_{f\_corr}$ (W m$^{-2}$K$^{-1}$) |
|---|---|---|---|---|---|---|---|---|---|
| 300 | 50 | 300,35 | 303,07 | 400 | 18516 | 9224 | 968,4 | 987,1 | 981,9 |
| 400 | 50 | 300,43 | 304,12 | 400 | 24688 | 12299 | 1317,5 | 1349,0 | 1342,5 |
| 500 | 50 | 300,50 | 304,97 | 400 | 30860 | 15374 | 1593,3 | 1638,6 | 1630,2 |
| 600 | 50 | 300,59 | 305,68 | 400 | 37032 | 18449 | 1813,0 | 1872,1 | 1861,0 |
| 700 | 50 | 300,67 | 306,38 | 400 | 43204 | 21523 | 2035,3 | 2110,2 | 2096,2 |
| 800 | 50 | 300,75 | 307,15 | 400 | 49376 | 24598 | 2282,3 | 2377,0 | 2359,2 |
| 900 | 50 | 300,83 | 307,88 | 400 | 55548 | 27673 | 2514,5 | 2630,1 | 2608,5 |
| 1000 | 50 | 300,91 | 308,37 | 400 | 61720 | 30748 | 2655,5 | 2786,0 | 2760,6 |
| 1200 | 50 | 301,04 | 309,72 | 400 | 74064 | 36897 | 3093,6 | 3271,6 | 3237,8 |

**Table 6.6 Results and calculations for simulations SST k-ω model with Production Limiter, Production Kato-Launder and intermittency Transition Model options activated, *h/d*=1**

| n (rpm) | Δt (s) | Tb-o (K) | Tb-f (K) | Tw (K) | Re-m (-) | Re (-) | $\alpha_f$ (W m$^{-2}$K$^{-1}$) | $\alpha_{IM}$ (W m$^{-2}$K$^{-1}$) | $\alpha_{f\_corr}$ (W m$^{-2}$K$^{-1}$) |
|---|---|---|---|---|---|---|---|---|---|
| 300 | 50 | 300,66 | 304,9 | 400 | 18516 | 9224 | 1516,7 | 1562,5 | 1550,2 |
| 400 | 50 | 300,59 | 306 | 400 | 24688 | 12299 | 1912,4 | 1977,5 | 1965,9 |
| 500 | 50 | 300,83 | 307,2 | 400 | 30860 | 15374 | 2261,0 | 2357,6 | 2336,6 |
| 600 | 50 | 300,86 | 308,2 | 400 | 37032 | 18449 | 2615,2 | 2742,5 | 2717,1 |
| 700 | 50 | 300,95 | 309,2 | 400 | 43204 | 21523 | 2951,3 | 3112,5 | 3082,0 |
| 800 | 50 | 301,03 | 310,2 | 400 | 49376 | 24598 | 3267,9 | 3465,4 | 3429,3 |
| 900 | 50 | 301,11 | 311,1 | 400 | 55548 | 27673 | 3563,7 | 3800,4 | 3757,0 |
| 1000 | 50 | 301,19 | 312 | 400 | 61720 | 30748 | 3845,9 | 4123,2 | 4072,7 |
| 1200 | 50 | 301,36 | 313,6 | 400 | 74064 | 36897 | 4344,7 | 4703,3 | 4637,7 |

The results of heat transfer coefficient at the bottom were plotted in order to have a better understanding of the values. Figure 6.4 shows the heat transfer coefficients, where it can be noticed that the values obtained by the intermittency Transition Model were around 1,5 higher than the ones without that option activated. In addition, it can be observed that by applying the correction factor described by Eq. (37), the values got closer to the ones calculated by the integral method. Therefore, the heat transfer coefficients obtained by the energy balance (integral method) were considered as the most accurate value and were used for the following results.
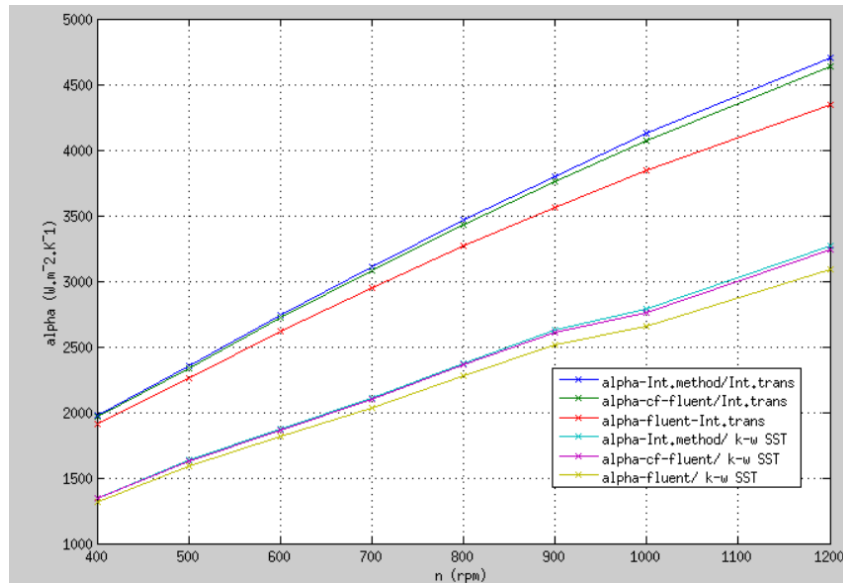


**Figure 6.4** Heat transfer coefficients by different methods and model options activated

A comparison between SST k- ω vs SST k- ω with intermittency Transition Model activated was performed to determine which method fits better with the published heat transfer correlations mentioned in chapter 3. As first step, Nusselt number, Eq. (7), was computed by using the heat transfer coefficients from integral method to replace in part of Eq. (8) (the commonly used value of 1/3 was kept as exponent of Prandtl number).

$$\frac{\text{Nu}}{\text{Pr}^{1/3}} = C \, \text{Re}_\text{m}{}^{p} \tag{39}$$

Then, the model parameters *C* and *p* were determined in MATLAB by applying 'nlinfit2' function. Nonlinear regression was performed for the 2 parameters, and the confidence interval was found. The following code was used for previous studies and was based on (Petera, 2016)

```
function [ a, resid, Jc, ci, cip, cipp ] =
nlinfit2(Xi,Yi,fmodel,Binit)

np = length(Binit);
if  (~ exist('OCTAVE_VERSION'))
  [a,resid,Jc,covb] = nlinfit(Xi,Yi,fmodel,Binit);
  ci = nlparci(a,resid,'jacobian',Jc,'alpha',1-0.95);
  cip = a' - ci(:,1);
else
  % leasqr in Octave expects opposite order of input
parameters
  fmodel2 = @(x,a) fmodel(a,x);
  [y2,a,kvg,iter,corp,covp,covr,stdresid,Z,r2] =
leasqr(Xi,Yi,Binit,fmodel2);
  %%beta = a;
  resid = Yi - y2; % residua
  N = length(Xi);
  nf = N-np;
  Sv2 = sum(resid.^2)/nf;
  %covp
  Jc = [];
  C = sum(stdresid.^2)/nf*covp;
  t975 = tinv(0.975,nf);
  for i=1:np;
    stde(i) = sqrt(C(i,i));
    cip(i) = stde(i)*t975;
    ci(i,:) = [a(i)-cip(i),a(i)+cip(i)];
  end
end

cipp = cip./abs(a')*100;
```

```
    for i=1:np;
      fprintf('beta(%d): %12f +- %10f (%.2f%%),   %12f ...
    %12f\n',i,a(i),cip(i),cipp(i),ci(i,:));
    end
```

The results obtained in MATLAB are summarized in Table 6.7. It is important to mention that the values corresponding to 300 rpm were discarded because the parameters $p$ were higher. The reason might be that the flow is not fully turbulent with 300 rpm ($Re_m$=18516).

**Table 6.7 Model parameters**

| Model | $C$ | Confidence interval | $p$ | Confidence interval |
|-------|-----|--------------------|-----|---------------------|
| **SST k-w without intermittency** | 0,0259 | ±31,83% | 0,7980 | ±3,67% |
| **SST k-w with intermittency** | 0,0422 | ±22,16% | 0,7877 | ±2,59% |

Next, the results were plotted to compare with correlations for heat transfer coefficient at the bottom of a cylindrical vessel described in chapter 3.

For the comparison, Equations (10) and (11) were used. Eq. (11) was expressed in terms of $Re_m$ without and with Swirl number included ($h/d$=1). Swirl number was computed by Eq. (12), Eq. (13) and values from Table 3.1. The correlations were expressed as follows:

$$\frac{\text{Nu}}{\text{Pr}^{1/3}} = 0{,}101 \, \text{Re}_m{}^{0{,}680} \tag{10}$$

$$\frac{\text{Nu}}{\text{Pr}^{1/3}} = 0{,}041 \left(\frac{4 \, d_m \, N_Q}{\pi \, d}\right)^{0{,}826} \text{Re}_m{}^{0{,}826} = 0{,}0231 \text{Re}_m{}^{0{,}826} \tag{40}$$

$$\frac{\text{Nu}}{\text{Pr}^{1/3}} = 0{,}041 \left(\frac{4 \, d_m \, N_Q}{\pi \, d}\right)^{0{,}826} \text{Re}_m{}^{0{,}826} \text{Sw}^{0{,}609} = 0{,}0186 \text{Re}_m{}^{0{,}826} \tag{41}$$

Figure 6.5 shows the results, where it can be noticed that values related to the intermittency Transition Model were higher than the correlations, while the values obtained by the energy balance without intermittency option activated have a good agreement with them. Therefore, the SST k-ω model with Production Limiter and Production Kato-Launder options activated was selected to continue the set of simulations for different position of the draft tube with respect to the vessel bottom.
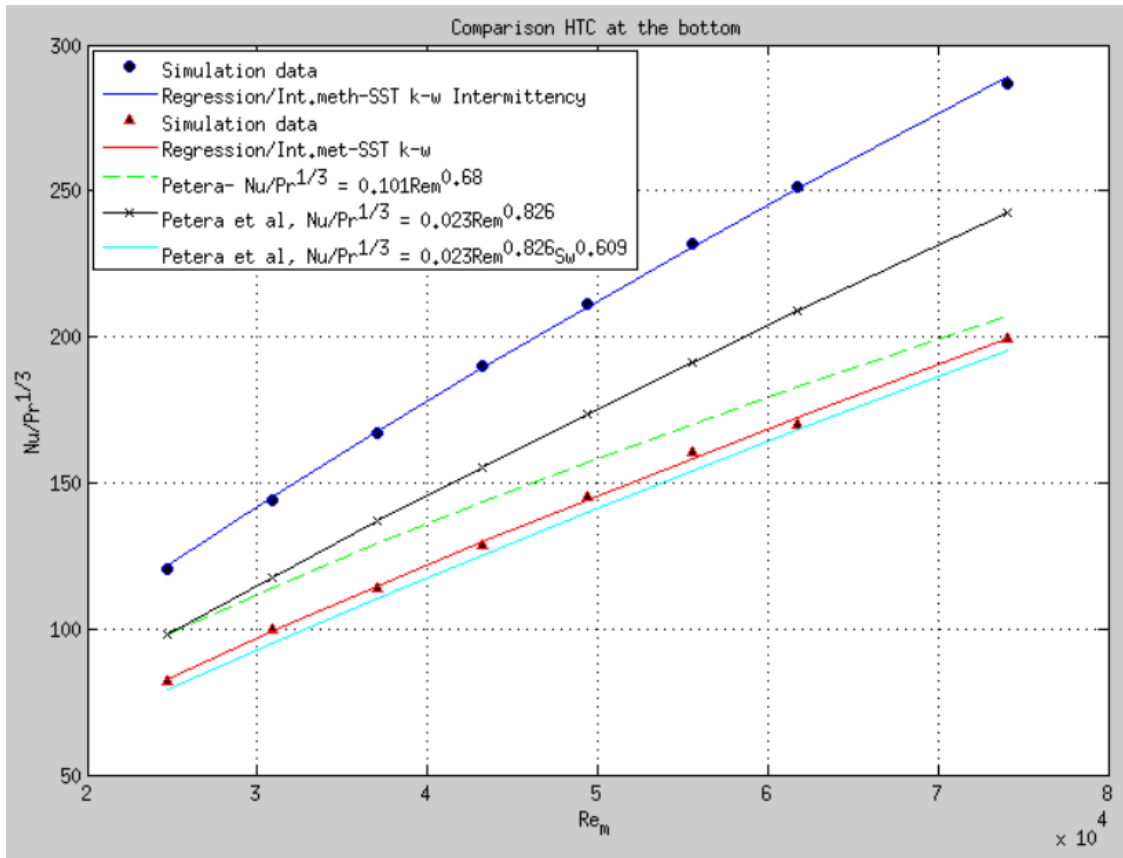
**Figure 6.5** Comparison SST k-ω model with and without Intermittency option activated vs Nu number correlations

## 6.3. Simulations for different position of the draft tube with respect to the vessel bottom

The last set of simulations were performed by applying the SST k-ω model with Production Limiter and Production Kato-Launder options activated for different position of the draft tube with respect to the vessel bottom ($h/d$ = 0,5 and 0,25). Same conditions as the ones used for $h/d$=1 were kept in the simulations.

The simulations were run until the convergence was obtained. The results are shown in Table 6.8 and Table 6.9, where the values were calculated by using the same methodology that was described in sections 6.1 and 6.2.

**Table 6.8 Results and calculations for simulations SST k-ω model with Production Limiter and Production Kato-Launder options activated, _h/d_=0,5**

| n (rpm) | $\Delta t$ (s) | Tb-o (K) | Tb-f (K) | Tw (K) | Re-m (-) | Re (-) | $\alpha_f$ (W m$^{-2}$K$^{-1}$) | $\alpha_{IM}$ (W m$^{-2}$K$^{-1}$) | $\alpha_{f\_corr}$ (W m$^{-2}$K$^{-1}$) |
|---|---|---|---|---|---|---|---|---|---|
| 300 | 50 | 300,42 | 304,04 | 400 | 18516 | 8690 | 1290,3 | 1320,1 | 1314,3 |
| 400 | 50 | 300,50 | 305,10 | 400 | 24688 | 11587 | 1637,4 | 1685,0 | 1676,4 |
| 500 | 50 | 300,61 | 305,96 | 400 | 30860 | 14484 | 1907,4 | 1972,7 | 1960,7 |
| 600 | 50 | 300,69 | 307,13 | 400 | 37032 | 17380 | 2295,1 | 2389,6 | 2372,9 |
| 700 | 50 | 300,82 | 308,08 | 400 | 43204 | 20277 | 2589,9 | 2712,0 | 2689,7 |
| 800 | 50 | 300,90 | 308,92 | 400 | 49376 | 23174 | 2858,1 | 3007,7 | 2980,4 |
| 900 | 50 | 301,01 | 309,99 | 400 | 55548 | 26071 | 3199,7 | 3388,6 | 3354,2 |
| 1000 | 50 | 301,10 | 310,78 | 400 | 61720 | 28967 | 3449,0 | 3670,2 | 3629,6 |
| 1200 | 50 | 301,28 | 312,43 | 400 | 74064 | 34761 | 3971,8 | 4269,3 | 4214,4 |

**Table 6.9 Results and calculations for simulations SST k-ω model with Production Limiter and Production Kato-Launder options activated, _h/d_=0,25**

| n (rpm) | $\Delta t$ (s) | Tb-o (K) | Tb-f (K) | Tw (K) | Re-m (-) | Re (-) | $\alpha_f$ (W m$^{-2}$K$^{-1}$) | $\alpha_{IM}$ (W m$^{-2}$K$^{-1}$) | $\alpha_{f\_corr}$ (W m$^{-2}$K$^{-1}$) |
|---|---|---|---|---|---|---|---|---|---|
| 300 | 50 | 300,46 | 304,55 | 400 | 18516 | 7581 | 1457,8 | 1496,2 | 1488,6 |
| 400 | 50 | 300,57 | 305,76 | 400 | 24688 | 10108 | 1848,5 | 1909,8 | 1898,5 |
| 500 | 50 | 300,68 | 306,92 | 400 | 30860 | 12635 | 2223,4 | 2312,4 | 2296,3 |
| 600 | 50 | 300,84 | 308,34 | 400 | 37032 | 15162 | 2672,8 | 2803,4 | 2779,3 |
| 700 | 50 | 300,92 | 309,27 | 400 | 43204 | 17689 | 2976,0 | 3138,1 | 3109,0 |
| 800 | 50 | 301,03 | 310,14 | 400 | 49376 | 20215 | 3245,4 | 3440,4 | 3404,6 |
| 900 | 50 | 301,11 | 311,24 | 400 | 55548 | 22742 | 3609,7 | 3851,2 | 3808,2 |
| 1000 | 50 | 301,24 | 312,29 | 400 | 61720 | 25269 | 3938,8 | 4229,8 | 4177,1 |
| 1200 | 50 | 301,45 | 314,19 | 400 | 74064 | 30323 | 4541,4 | 4935,0 | 4863,1 |

The results of the 3 set of simulations (_h/d_=1, 0,5 and 0,25) are shown in Figure 6.6. It can be observed that the heat transfer coefficients are higher for the relation _h/d_=0,25 because the draft tube is closer to the bottom of the tank, which for this case is the source of heat. Comparing to the relation _h/d_=1, the values were 1,28 times and 1,47 times higher for _h/d_=0,5 and 0,25 respectively as average. Moreover, the effect of the correction factor Eq. (37) is clearly visible here as it was explained previously.
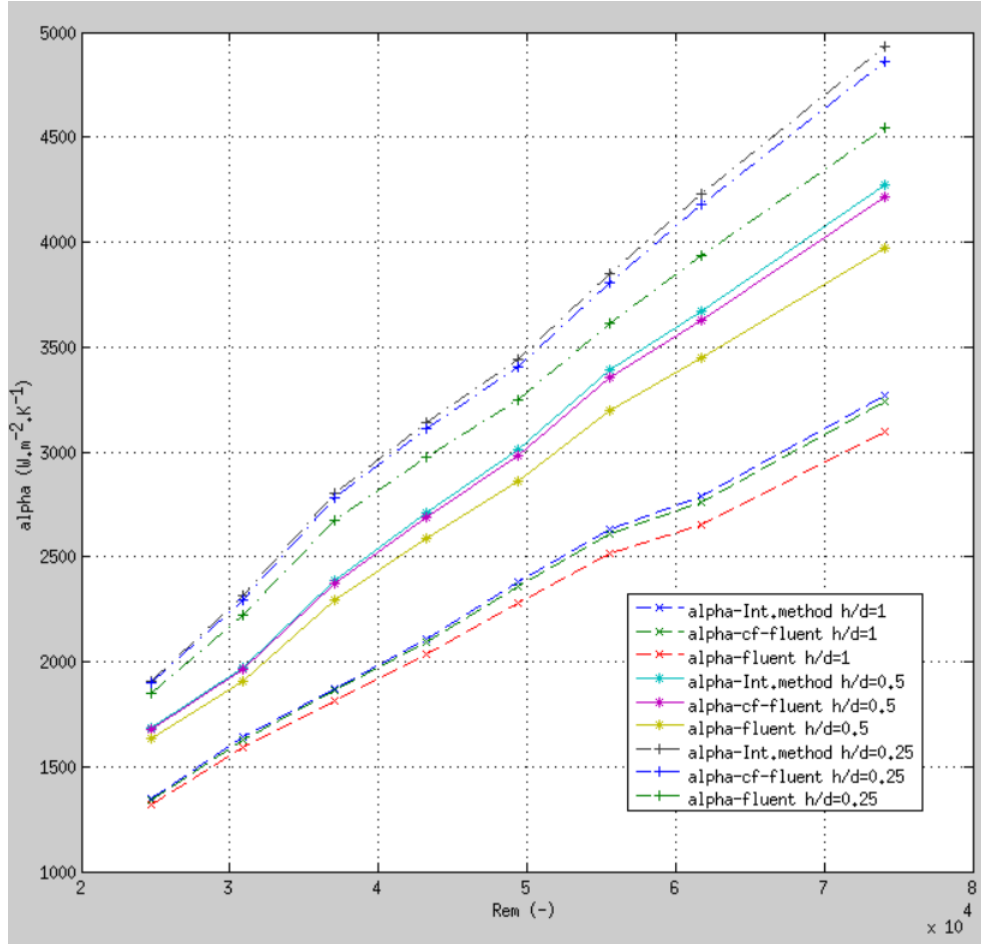
**Figure 6.6** Heat transfer coefficients for different position of the draft tube with respect to the vessel bottom

Besides, the following analysis was done to find out if a relationship between Swirl (Sw) and Reynolds (Re) numbers exists here. For this purpose, the F-test was used to determine if Swirl number has a dependence on Reynolds number (alternative hypothesis), or if it is a constant value (null hypothesis). Swirl number was expressed by Eq.(42), which is the relation between the axial flux of tangential momentum and the axial flux of axial momentum (Chigier et al., 1964) .

$$Sw = \frac{2\,G_w}{d\,G_u} \tag{42}$$

Where:

$G_w$      axial flux of tangential momentum (kg m$^2$ s$^{-1}$)

$G_u$       axial flux of axial momentum (kg m$^2$ s$^{-1}$)

The values for $G_w$ and $\frac{d}{2}G_u$ were obtained from ANSYS-Fluent and are shown in Table 6.10.

**Table 6.10 Swirl number for different position of the draft tube with respect to the vessel bottom**

| n | h/d=1 | | | h/d=0,5 | | | h/d=0,25 | | |
|---|---|---|---|---|---|---|---|---|---|
| (rpm) | $G_w$ | d/2 $G_u$ | Sw | $G_w$ | d/2 $G_u$ | Sw | $G_w$ | d/2 $G_u$ | Sw |
| 400 | 6,13e-06 | 4,50e-06 | 1,361 | 6,29e-06 | 5,10e-06 | 1,235 | 5,70e-06 | 4,34e-06 | 1,314 |
| 500 | 9,86e-06 | 7,46e-06 | 1,323 | 9,56e-06 | 7,65e-06 | 1,250 | 9,04e-06 | 6,94e-06 | 1,303 |
| 600 | 1,41e-05 | 1,05e-05 | 1,341 | 1,46e-05 | 1,22e-05 | 1,202 | 1,30e-05 | 1,13e-05 | 1,156 |
| 700 | 1,92e-05 | 1,42e-05 | 1,348 | 1,95e-05 | 1,61e-05 | 1,209 | 1,80e-05 | 1,45e-05 | 1,238 |
| 800 | 2,56e-05 | 1,91e-05 | 1,339 | 2,57e-05 | 2,08e-05 | 1,237 | 2,36e-05 | 1,80e-05 | 1,311 |
| 900 | 3,27e-05 | 2,45e-05 | 1,334 | 3,34e-05 | 2,82e-05 | 1,185 | 3,02e-05 | 2,35e-05 | 1,287 |
| 1000 | 3,94e-05 | 2,83e-05 | 1,391 | 4,10e-05 | 3,32e-05 | 1,236 | 3,75e-05 | 2,92e-05 | 1,283 |
| 1200 | 5,79e-05 | 4,14e-05 | 1,397 | 5,95e-05 | 4,68e-05 | 1,272 | 5,47e-05 | 4,15e-05 | 1,317 |

Next, the F-test was performed to find out the alternative hypothesis or the null hypothesis ($p$=0). Reynolds number and Swirl number were described by the following form:

$$Sw = C_1 \, Re^p \qquad\qquad (43)$$

Where $C_1$ and $p$ are the model parameters. $C_1$ and $p$ were computed in MATLAB by 'nlinfit' function (based on least squares method), which is part of the following 'ftest' function. This function allows to find out if the model parameter $p$ is near to zero or there is a significant difference from the null hypothesis. The 'ftest' function is shown below (Petera, 2016):

```
function [beta,beta0]=ftest(Re,Sw)
%F test
Re;
Sw;
fmodel = @(beta,x) beta(1)*x.^beta(2); %alt.model
[beta,resid,J]= nlinfit(Re,Sw,fmodel, [1 1]);
fmodel0 = @(beta,x) beta(1)*x.^0; %nul.model
[beta0,resid0,J0]= nlinfit(Re,Sw,fmodel0, [1 1]);
nn=length(Re);
SSnul = sum(resid0.^2) %null hypothesis - 1 param
```

```
SSalt = sum(resid.^2) %alternate model - 2 para
DFnul = nn-1;
DFalt = nn-2;
F = (SSnul-SSalt)/SSalt / ((DFnul-DFalt)/DFalt)
Fcrit = finv(0.95, DFnul-DFalt, DFalt)
Pr = fcdf(F,DFnul-DFalt, DFalt)
p = 1-Pr
if (F>Fcrit) %if (p<= 0.05)
    fprintf('significant difference, F>Fcrit p<0.05,\n');
else
    fprintf('not significant difference, F<Fcrit
p>0.05,\n');
end
```

As a result, the obtained parameter *p* was 0,0292, which means that there is not significant dependency between Re and Sw numbers. Therefore, Swirl number was considered as a constant value that will be part of the *C* model parameter in the final correlation. The influence of tangential velocity component could not be determined by this technique. To illustrate, Figure 6.7 shows Reynolds vs Swirl numbers plot.
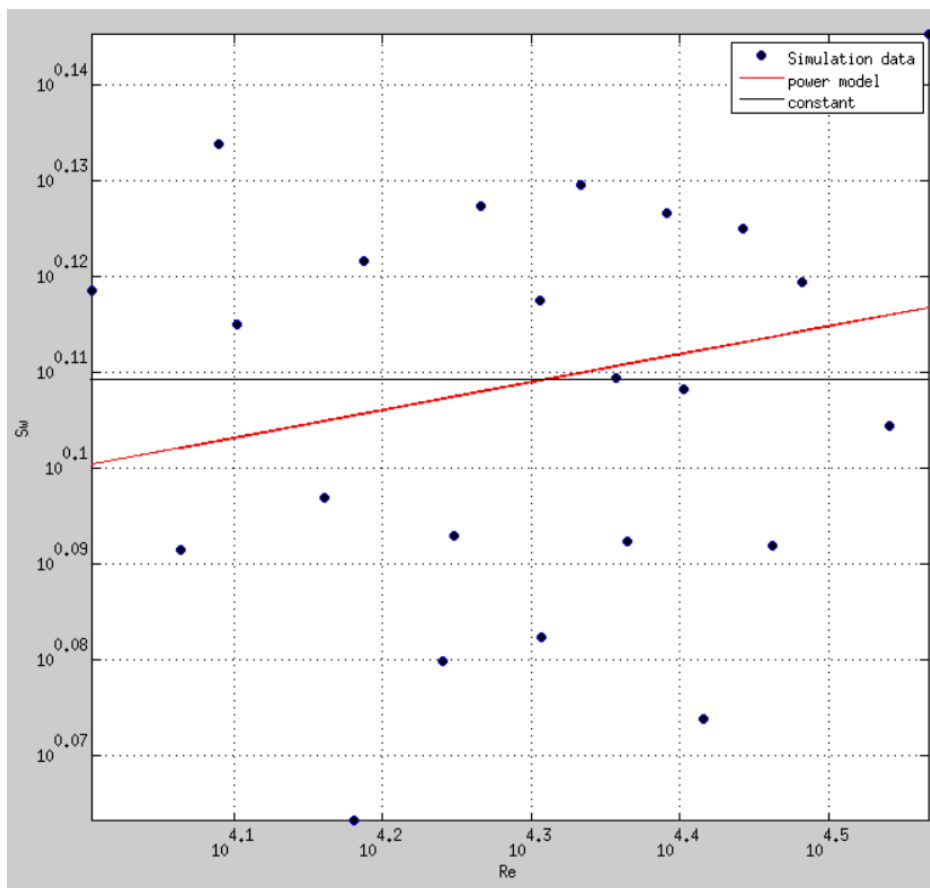


**Figure 6.7** Swirl number vs Reynolds number

40

## 6.4. Determination of Nusselt number correlation

A similar procedure described in subchapter 6.2 was used to determine the model parameters. For this case $C$, $p$ and $s$, based on part of Eq. (11)

$$\frac{\text{Nu}}{\text{Pr}^{1/3}} = C \, \text{Re}_\text{m}{}^{p} \left(\frac{h}{d}\right)^{s}$$

(44)

From the results of the simulations described in previous sections for $h/d$=1, 0,5 and 0,25, Nusselt number was computed by Eq. (7). Next, the model parameters $C$, $p$ and $s$ were determined in MATLAB by applying nonlinear regression for multiple independent variables with the 'nlinfit2' function as it was described previously. The results are shown in Table 6.11, where the confidence interval of the model parameter $C$ was 46,5%. This value depends on many factors, for example the Swirl number, which may influence in the wide confidence interval.

**Table 6.11 Model parameters for Nusselt number correlation**

| $C$ | Confidence interval | $p$ | Confidence interval | $s$ | Confidence interval |
|---|---|---|---|---|---|
| 0,0164 | ±46,46% | 0,8426 | ±5,06% | -0,274 | ±8,46% |

Consequently, the correlation obtained based on the heat transfer coefficient by the energy balance (integral method) is described as follows:

$$\overline{\text{Nu}} = 0,0164 \, \text{Re}_\text{m}{}^{0,843} \, \text{Pr}^{1/3} \left(\frac{h}{d}\right)^{-0,274}$$

(45)

Eq. (45) describes the heat transfer coefficient at the bottom of an agitated vessel with an axial 6-blade impeller (pitched angle 45º) placed in a draft tube. This equation is valid for $10000 < \text{Re} < 40000$ or $20000 < \text{Re}_\text{m} < 80000$ and $0,25 \leq h/d \leq 1$.

The obtained correlation was compared with published correlations Eq. (10), Eq. (11) and Eq. (49). The last one is the result obtained with Sliding Mesh approach (Calvopina, 2018). All of them were described in terms of $\text{Re}_\text{m}$, which were derived from Eq. (11) and by using Eq. (5) for the different $h/d$. Swirl number was computed by Eq. (12), Eq. (13) and values from Table 3.1:

$$\frac{\text{Nu}}{\text{Pr}^{1/3}} = 0{,}101 \ \text{Re}_\text{m}{}^{0{,}680} \tag{10}$$

$$\frac{\text{Nu}}{\text{Pr}^{1/3}} = 0{,}041 \ \text{Re}^{0{,}826} \left(\frac{h}{d}\right)^{-0{,}099} \text{Sw}^{0{,}609} \tag{11}$$

$$\frac{h}{d} = 1 \rightarrow \frac{\text{Nu}}{\text{Pr}^{1/3}} = 0{,}0231 \text{Re}_\text{m}{}^{0{,}826} \left(\frac{h}{d}\right)^{-0{,}099} \text{Sw}^{0{,}609} \tag{46}$$

$$\frac{h}{d} = 0{,}5 \rightarrow \frac{\text{Nu}}{\text{Pr}^{1/3}} = 0{,}0219 \text{Re}_\text{m}{}^{0{,}826} \left(\frac{h}{d}\right)^{-0{,}099} \text{Sw}^{0{,}609} \tag{47}$$

$$\frac{h}{d} = 0{,}25 \rightarrow \frac{\text{Nu}}{\text{Pr}^{1/3}} = 0{,}0196 \text{Re}_\text{m}{}^{0{,}826} \left(\frac{h}{d}\right)^{-0{,}099} \text{Sw}^{0{,}609} \tag{48}$$

$$\frac{\text{Nu}}{\text{Pr}^{1/3}} = 0{,}002 \ \text{Re}^{1{,}059} \tag{49}$$

$$\frac{h}{d} = 1 \rightarrow \frac{\text{Nu}}{\text{Pr}^{1/3}} = 0{,}001 \text{Re}_\text{m}{}^{1{,}059} \tag{50}$$

Finally, the comparisons for different position of the draft tube with respect to the vessel bottom are shown in Figures 6.8, 6.9 and 6.10, where it can be noticed a good agreement with the published correlations. However, bigger differences are visible when the ratio *h/d* is reduced. In addition, Figures 6.8 shows that the result obtained in this work with MRF approach fits better than the one obtained in previous study with Sliding Mesh approach (Calvopina, 2018) compared to experimental data.

The MATLAB script used for this study is attached in Appendix A.
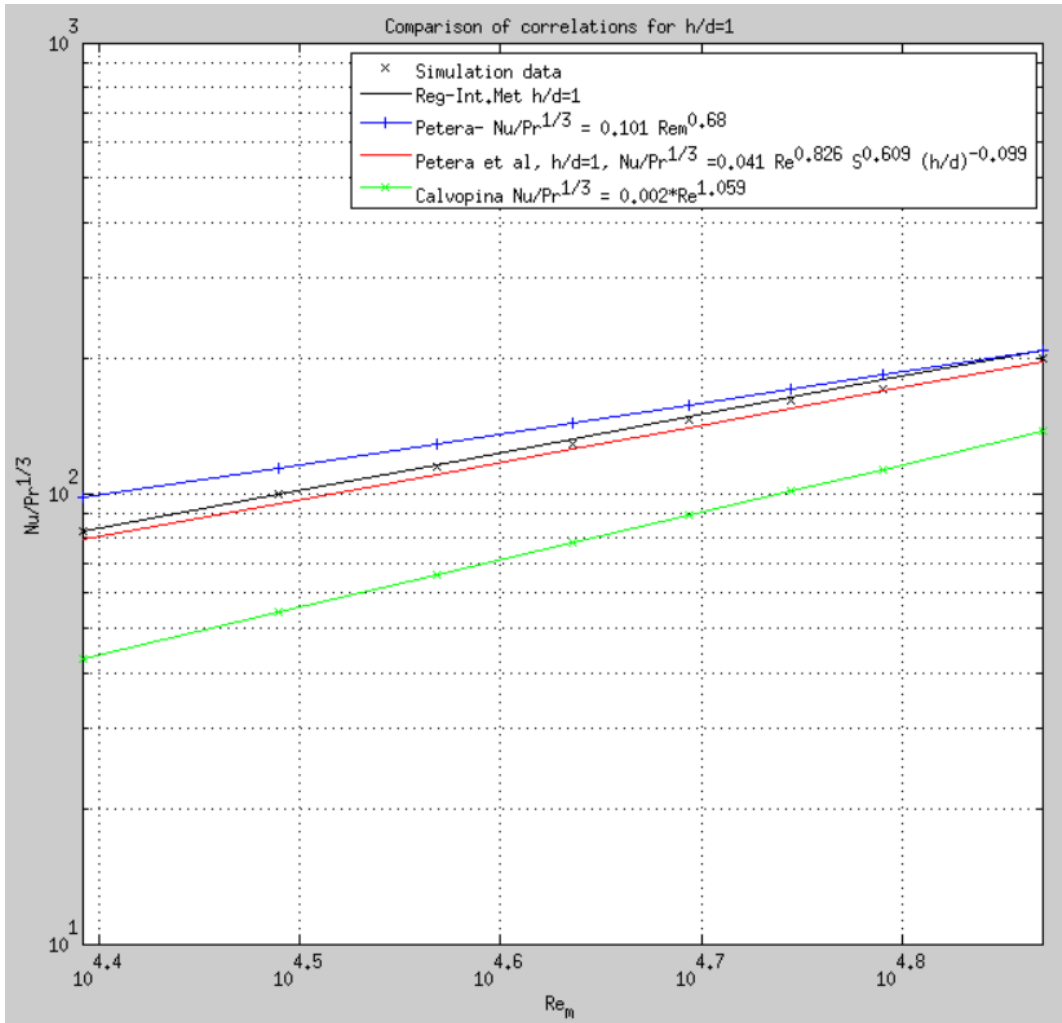
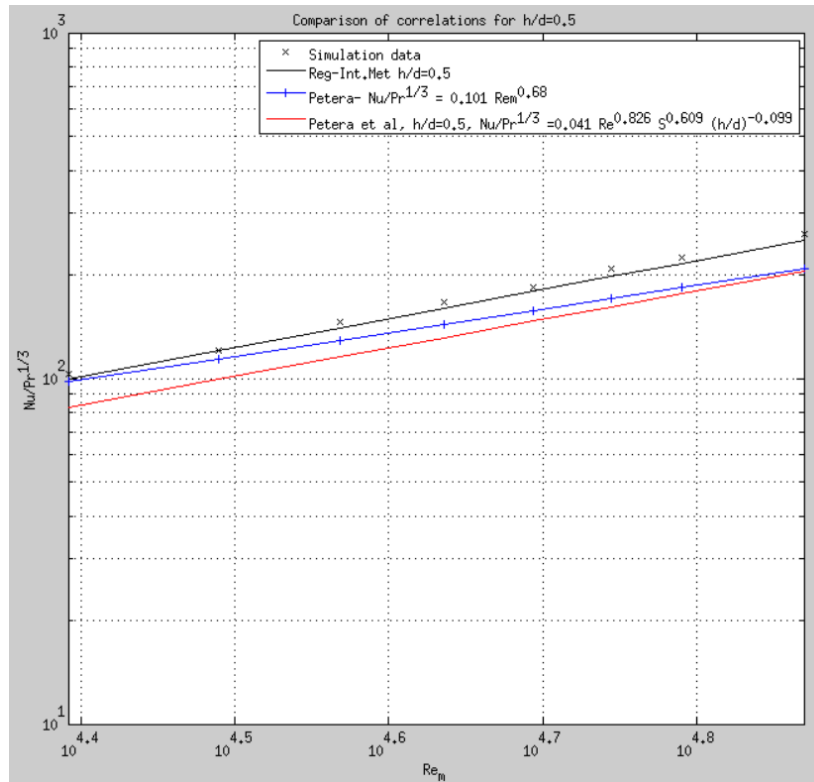**Figure 6.8** Comparison of correlations for *h/d*=1

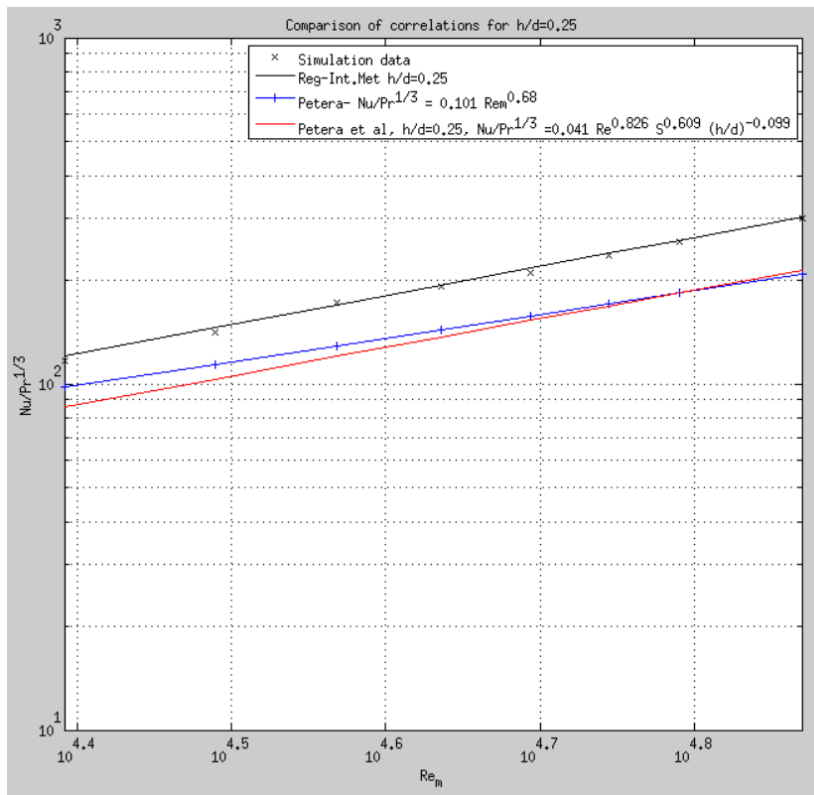**Figure 6.9** Comparison of correlations for *h/d*=0,5



**Figure 6.10** Comparison of correlations for *h/d*=0,25

# Chapter 7.    Conclusions and Further scope

The CFD analysis of heat transfer in an agitated vessel with a draft tube was performed in order to obtain a correlation for heat transfer at the bottom of the tank. The following conclusions are summarized here:

- Based on literature research, correlations by (Petera, 2017) and (Petera et al., 2017) were published for this specific geometry. They implied that there is similarity in the working principle between the flow generated by the axial impeller inside the draft tube and impinging jets. Therefore, they were selected to compare with the results of this study.

- The given mesh applied in the current project was examined finding out that the mesh metrics fit under recommended range values to obtain accurate results.

- The first simulations, run in ANSYS-Fluent, were done for different intervals from 0 to 200 seconds with constant rotational speed in order to find out the simulated time which gives reasonable accuracy. The SST k-ω model was applied using MRF approach which is less computationally demanding compared with Sliding Mesh.

- From the first simulations, 2 different heat transfer coefficients were obtained. The first one was retrieved directly from Fluent, and the other was calculated by using energy balance equation. A correction factor was applied to the first one to avoid an inaccuracy produced by the program that keeps the reference temperature of the fluid constant while the time goes on. From that comparison, the heat transfer coefficient obtained by the energy balance was chosen for the further analysis because it is more precise. In addition, it was determined that 50 seconds will be the time for the subsequent simulations because there was a slight variation of the heat transfer coefficients after that time.

- The next set of simulations for different rotational speed were run, and a comparison of SST k-ω model with and without intermittency Transition Model option activated was performed. The results were compared with the published correlations obtaining that the simulations without intermittency had a better

agreement. Therefore, the SST k-ω model with Production Limiter and Production Kato-Launder options activated was used in the next simulations.

- The following set of simulations were run for different position of the draft tube with respect to the vessel bottom. As a result, a Nusselt correlation for the bottom of the tank was obtained. This correlation describes the Nusselt number in terms of the Reynolds and Prandtl numbers and dimensionless distance (*h/d*). The influence of Swirl number was found as a constant.

- The correlation was compared with published correlations obtaining good agreement for *h/d*=1, but bigger differences were visible when *h/d* decreased.

- Despite the MRF approach used in this work, the results are in better agreement compared with experimental data than the results obtained with Sliding Mesh approach (Calvopina, 2018). This is mainly the consequence of the length of simulated time range. With the Sliding mesh, much smaller time steps are required; therefore, substantially larger number of time steps and consequently larger computational requirements are necessary to get results for the same simulated time. The computational requirements with MRF approach are much smaller which provides the possibility to increase the simulated time range as well as to perform simulations over wider range of parameters.

Based on the idea that there is a similarity in the working principle between impinging jets and the flow generated by the axial impeller with a draft tube, Nusselt correlations were obtained in previous research. From this statement, the current study was performed to obtain a correlation for heat transfer at the bottom of the tank. However, further research can be carried out because only few studies have been related to this topic.

- Additional experimental data can be measured to be compared with the published correlations. Then, research for heat transfer at the vessel walls can be performed to find a correlation.

- Emphasize the Swirl dependency by getting a better understanding of its influence by additional literature resarch and different methods.

- Sieder-Tate effect can be included to get more accurate results when the temperature diffrence between the working fluid and the heating/coolong fluid is high.

- Additional simuations can be performed with different turbulent models to determine if better results can be obtained.

# References

**ANSYS 15.0 Training Materials.** *Heat Transfer.* Prague : ANSYS, 2013.

**ANSYS 15.0 Training Materials.** *Turbulence Modeling.* Prague : ANSYS, 2013.

**ANSYS, INC.** *ANSYS Fluent Theory Guide.* Canonsburg, : ANSYS, 2013. Release 15.0.

**Calvopina, H.** *CFD simulation of heat transfer in an agitated vessel with a draft tube.* Prague : Czech Technical University in Prague, 2018. Master's Thesis.

**Chakravarty, A.** *CFD Simulation of Heat Transfer in an Agitated Vessel.* Prague : Czech Technical University in Prague, 2017. Master's Thesis.

**Chigier, N. A, Beér, J. M.** *Velocity and static-pressure distributions in swirling air jets issuing from annular and divergent nozzles.* s.l. : Journal of Basic Engineering, ASME, 1964. Vol. 86.

**Couper, J., Penney, R., Fair, J., Walas, S.** *Chemical Process Equipment, Selection and Design.* Burlington : Gulf Professional Publishing, 2005. p. 283. 978-0-7506-7510-9.

**Jirout, T., Vlček, P.** *CFD simulation of flow in mixing equipment with draft tube.* Czech Republic : CHISA conference, 2015.

**Kresta, S., Etchells, A., Dickey, D., Atiemo-Obeng, V. 2016.** *Advances in Industrial Mixing.* Hoboken : John Wiley & Sons, Inc, 2016. p. 123. 978-0-470-52382-7.

**Kundu, P., Cohen, I., Dowling, D.** *Fluid Mechanics.* Waltham : Elsevier Inc., 2016. 978-0-12-405935-1.

**Langel, C., Chow, R.,Van Dam, C.** *A Comparison of Transition Prediction Methodologies Applied to High Reynolds Number External Flows.* Davis : University of California, 2016.

**Paul, E., Atiemo, V., Kresta, S.** *Handbook of industrial mixing, Science and Practice.* New Jersey : John Wiley & Sons, Inc., Hoboken, 2004. pp. 345-351. 0471269190.

**Persoons, T., McGuinn, A., Murray, D.** *A general correlation for the stagnation point Nusselt number.* s.l. : International Journal of Heat and Mass Transfer, 2011. Vol. 54.

**Petera, K.** *Habilitation Thesis.* Faculty of Mechanical Engineering, CTU Prague. Prague : Czech Technical University, 2017.

**Petera, K.** Linear and Non linear regression. Prague : Czech Technical University, 2016.

**Petera, K.** Tutorial Momentum Heat and Mass Transfer. Prague : Czech Technical University in Prague, 2017.

**Petera, K., Dostál, M., Věříšová, M., Jirout, T.** *Heat Transfer at the Bottom of a Cylindrical Vessel Impinged by a Swirling Flow from an Impeller in a Draft Tube.* Zagreb : Chemical and Biochemical Engineering Quarterly, 2017. pp. 343-352. Vol. 31 (3) (2017). 10.15255/CABEQ.2016.1057.

# Appendix A.

# MATLAB script

```matlab
di = 0.07; % (m) diameter of the draft tube

dm = 0.061; % (m) diameter of the impeller

D = 0.392; % (m) diameter of the tank

H = 0.43; % (m) height of the tank


rho = 998.2; %(kg.m-3)

mu = 0.001003; nu = mu/rho;

lambda_f = 0.6; cp = 4182;

a=lambda_f/(rho*cp); % thermal diffusivity

Pr = nu/a;

Pr3 = Pr^(1/3);

n=[300:100:1000 1200];

h_d=[1 0.5 0.25];

Nq= [0.449 0.423 0.369]'; %Pump capacity pitched angle 45

Wstar=[0.1817 0.1786 0.1789]; %dimensionless tang velocities

W_U=(pi()*di/(2*dm))^2*(Wstar./Nq');

S=8/15*W_U;


%Intermittency Trans model
alpha_int_tr =

[1562.482972 1977.508634 2357.573062 2742.478438 3112.507521
3465.392864 3800.418732 4123.164427 4703.259466; %alpha int meth

1550.153898 1965.904573 2336.582067 2717.144478 3082.016667
3429.330339 3757.041305 4072.686657 4637.709848; %alpha-corr

   1516.67 1912.36 2260.98 2615.24 2951.27 3267.89 3563.67 3845.94
   4344.73]; %alpha_fluent
```

```
%SST k-w Kato-Launder

%h/d=1

alpha_kw_SST_d1 =

[987.1028108 1348.953464 1638.556846 1872.11444 2110.226781
2376.99281    2630.080622 2786.005572 3271.58; %alpha int meth

981.9180783 1342.544185 1630.17632    1861.018486 2096.192079
2359.208258   2608.461512 2760.612938 3237.800623; %alpha-corr

968.45 1317.46 1593.27 1812.99 2035.34 2282.26 2514.54 2655.47
3093.64]; %alpha_fluent

%h/d=0.5

alpha_kw_SST_d5 =

[1320.123757 1685.014759   1972.738694 2389.57061  2712.002538
3007.671894    3388.613927 3670.200174 4269.32; %alpha int meth

1314.339373    1676.410594 1960.665727 2372.922627 2689.674992
2980.374486    3354.220363 3629.59371  4214.434524; %alpha-corr

1290.30  1637.40    1907.39    2295.12    2589.89    2858.08
     3199.70 3448.96    3971.80]; %alpha_fluent

%h/d=0.25

alpha_kw_SST_d25 =

[1496.192639   1909.823267 2312.396489 2803.362477 3138.139995
3440.355721    3851.164717 4229.766349 4934.96; %alpha int meth

1488.59094     1898.450524 2296.261461 2779.285406 3108.972097
3404.596298    3808.184945 4177.122689 4863.064582; %alpha-corr

1457.78  1848.48    2223.36    2672.79    2976.03    3245.44
3609.65  3938.78    4541.40]; %alpha_fluent



i = 1:length(n);

i = 2:length(n);

n = n(i)

alpha=

[alpha_int_tr; alpha_kw_SST_d1; alpha_kw_SST_d5; alpha_kw_SST_d25];
```

```
alpha = alpha(:,i);

Rem = n./60.*dm^2/nu;

Lchar=di;

Re = Nq*Rem*4*dm/(pi()*di);

Sw=[1.448689741      1.361102287 1.323189993 1.340718938 1.347805037
       1.338508115    1.333637836 1.390900277 1.397225854; %h/d=1

     1.248425526      1.234620363 1.250151353 1.20171633  1.208736065
       1.236810445 1.185354881    1.235701409 1.271761372; %h/d=0.5

     1.313321168      1.314058175 1.303399777 1.156479702 1.2384785
       1.310977774    1.286544785 1.283131964 1.316584567]; %h/d=0.25

Sw= Sw(:,i);

Nu_cal = alpha.*Lchar/lambda_f;

Num_Pr = Nu_cal/Pr3; %Nu/Pr^1/3 at the bottom



% Comparison between SST k-w vs SST k-w with intermittency
   Transition Model activated

figure(1)

plot(n,alpha(1:6,:),'x-','MarkerFaceColor',[0 0 0]);

xlabel('n (rpm)')

ylabel('alpha (W.m^-2.K^-1)')

grid on;

legend('alpha-Int.method/Int.trans','alpha-cf-
   fluent/Int.trans','alpha-fluent-Int.trans','alpha-Int.method/ k-w
   SST','alpha-cf-fluent/ k-w SST','alpha-fluent/ k-w SST');



%Correlations

%NuPr = 0.023*Rem.^0.8; %Dittus-Boelter correlation

NuPr1 = 0.101*Rem.^0.68; %K. Petera- Hab Thesis

%NuPr2 = 0.041*Re.^0.826;  NuPr2 = 0.023*Rem.^0.826; %K. Petera et
   al, Heat Transfer at

NuPr2 = 0.041*(4*dm*(Nq*Rem)/(pi()*di)).^0.826; %K. Petera et al,
   Heat Transfer at
```

```
%NuPr3 = 0.041*Re.^0.826*S^0.609;  NuPr3 = (0.023 0.021
   0.0196)*Rem.^0.826*S^0.609; %K. Petera et al, Heat Transfer at

NuPr3 = (diag(S).^0.609)*0.041*(4*dm*(Nq*Rem)/(pi()*di)).^0.826; %K.
   Petera et al, Heat Transfer at

%NuPr4 = 0.041*Re.^0.826*S^0.609*(h/d)^-0.099;
   0.041*(4*dm*Nq/(pi()*di)^0.826*Rem.^0.826; %K. Petera et al,
   Heat Transfer at

NuPr4 = (diag((h_d).^-
   0.099))*(diag(S).^0.609)*0.041*(4*dm*(Nq*Rem)/(pi()*di)).^0.826;
   %K. Petera et al, Heat Transfer at

%NuPr5 = 0.002*Re.^1.059; %Calvopina

NuPr5 = 0.002*(4*dm*(Nq(1).*Rem)/(pi()*di)).^1.059;
```

**%Model function, model parameters C and p**

```
fmodel = @(c,R) c(1)*R.^c(2);%alpha int meth h/d=1, SST k-w with
   intermittency

[c1,r,J] = nlinfit2(Rem,Num_Pr(1,:),fmodel,[1 1]);

c1

NuPrbottom1 = c1(1)*Rem.^c1(2);



fmodel = @(c,R) c(1)*R.^c(2);

[c2,r,J] = nlinfit2(Rem,Num_Pr(2,:),fmodel,[1 1]);

c2

NuPrbottom2 = c2(1)*Rem.^c2(2);



fmodel = @(c,R) c(1)*R.^c(2);

[c3,r,J] = nlinfit2(Rem,Num_Pr(3,:),fmodel,[1 1]);

c3

NuPrbottom3 = c3(1)*Rem.^c3(2);



fmodel = @(c,R) c(1)*R.^c(2); %alpha int meth h/d=1, SST k-w
```

```
[c4,r,J] = nlinfit2(Rem,Num_Pr(4,:),fmodel,[1 1]);

c4

NuPrbottom4 = c4(1)*Rem.^c4(2);


fmodel = @(c,R) c(1)*R.^c(2);

[c5,r,J] = nlinfit2(Rem,Num_Pr(5,:),fmodel,[1 1]);

c5

NuPrbottom5 = c5(1)*Rem.^c5(2);


fmodel = @(c,R) c(1)*R.^c(2);

[c6,r,J] = nlinfit2(Rem,Num_Pr(6,:),fmodel,[1 1]);

c6

NuPrbottom6 = c6(1)*Rem.^c6(2);


fmodel = @(c,R) c(1)*R.^c(2); %alpha int meth h/d=0.5, SST k-w

[c7,r,J] = nlinfit2(Rem,Num_Pr(7,:),fmodel,[1 1]);

c7

NuPrbottom7 = c7(1)*Rem.^c7(2);


fmodel = @(c,R) c(1)*R.^c(2);

[c8,r,J] = nlinfit2(Rem,Num_Pr(8,:),fmodel,[1 1]);

c8

NuPrbottom8 = c8(1)*Rem.^c8(2);


fmodel = @(c,R) c(1)*R.^c(2);

[c9,r,J] = nlinfit2(Rem,Num_Pr(9,:),fmodel,[1 1]);

c9

NuPrbottom9 = c9(1)*Rem.^c9(2);
```

```matlab
fmodel = @(c,R) c(1)*R.^c(2); %alpha int meth h/d=0.25, SST k-w

[c10,r,J] = nlinfit2(Rem,Num_Pr(10,:),fmodel,[1 1]);

c10

NuPrbottom10 = c10(1)*Rem.^c10(2);


fmodel = @(c,R) c(1)*R.^c(2);

[c11,r,J] = nlinfit2(Rem,Num_Pr(11,:),fmodel,[1 1]);

c11

NuPrbottom11 = c11(1)*Rem.^c11(2);


fmodel = @(c,R) c(1)*R.^c(2);

[c12,r,J] = nlinfit2(Rem,Num_Pr(12,:),fmodel,[1 1]);

c12

NuPrbottom12 = c12(1)*Rem.^c12(2);


% Comparison SST k-w with and without Intermittency option activated
    vs Nu number correlations

figure(2)

plot(Rem,Num_Pr(1,:),'ob', Rem,NuPrbottom1,'b',Rem,Num_Pr(4,:),'^r',
    Rem,NuPrbottom4,'r', Rem,NuPr1,'g--', Rem,NuPr2(1,:),'kx-',
    Rem,NuPr3(1,:),'c-', 'MarkerFaceColor',[0 0 0]);

xlabel('Re_m')

ylabel('Nu/Pr^1^/^3')

grid on;

title ('Comparison HTC at the bottom')

legend('Simulation data','Regression/Int.meth-SST k-w
    Intermittency','Simulation data','Regression/Int.met-SST k-w',
    'Petera- Nu/Pr^1^/^3 = 0.101Rem^0^.^6^8',
    'Petera et al,Nu/Pr^1^/^3 = 0.023Rem^0^.^8^2^6',
    'Petera et al, Nu/Pr^1^/^3 = 0.023Rem^0^.^8^2^6Sw^0^.^6^0^9');
```

```matlab
% Comparison heat transfer coefficients for different h/d

figure(3)

plot(Rem,alpha(4:6,:),'x--',Rem,alpha(7:9,:),'*-
    ',Rem,alpha(10:12,:),'+-.','MarkerFaceColor',[0 0 0]);

xlabel('Rem (-)')

ylabel('alpha (W.m^-^2.K^-^1)')

grid on;

legend('alpha-Int.method h/d=1','alpha-cf-fluent h/d=1','alpha-
    fluent h/d=1','alpha-Int.method h/d=0.5','alpha-cf-fluent
    h/d=0.5','alpha-fluent h/d=0.5',
    'alpha-Int.method h/d=0.25','alpha-cf-fluent h/d=0.25',
    'alpha-fluent h/d=0.25');



% Swirl number dependence

xs=[Re(1,:)' Sw(1,:)';

    Re(2,:)' Sw(2,:)';

    Re(3,:)' Sw(3,:)'];



Rr=xs(:,1);



%F test

[alt,nul]=ftest(xs(:,1),xs(:,2));

alt;

nul;



fmodel = @(d,Rr) d(1).*Rr.^d(2);

[d1,r,J] = nlinfit2(Rr,xs(:,2),fmodel,[1 1]);

d1

Sw_1sst = d1(1)*xs(:,1).^d1(2);
```

56

```matlab
figure(4)

loglog(xs(:,1),xs(:,2),'ob',xs(:,1),Sw_1sst,'r',xs(:,1),nul(1),'k-',
    'MarkerFaceColor',[0 0 0]);

xlabel('Re')

ylabel('Sw')

grid on;

legend('Simulation data','power model','constant');


%Determination of Nusselt number correlation Nu=f(Re,Pr,h/d)

y = [Num_Pr(4,:)'; Num_Pr(7,:)'; Num_Pr(10,:)'];

Ry=[Rem';Rem';Rem'];


hd=[1 1 1 1 1 1 1 1;

    0.5 0.5 0.5 0.5 0.5 0.5 0.5 0.5;

    0.25 0.25 0.25 0.25 0.25 0.25 0.25 0.25];


x0=[Re(1,:)' hd(1,:)';

    Re(2,:)' hd(2,:)';

    Re(3,:)' hd(3,:)'];


x1=[Ry x0(:,2)];

%Model function, model parameters C, p, s

fmodel = @(g,x1) g(1)*x1(:,1).^g(2).*x1(:,2).^g(3);

[g1,r,J] = nlinfit2(x1,y,fmodel,[1 1 1 ]);

g1

Nu_Prc1 =g1(1)*x1(:,1).^g1(2).*x1(:,2).^g1(3);

NuPrcor1 = reshape(Nu_Prc1,[8,3])';

figure(5)
```

```
loglog(Rem,Num_Pr(4,:),'xk', Rem,NuPrcor1(1,:),'k', Rem,NuPr1,'b-
+',Rem,NuPr4(1,:),'r-',Rem,NuPr5,'g-x', 'MarkerFaceColor',[0 0 0]);

xlabel('Re_m')

ylabel('Nu/Pr^1^/^3')

grid on;

title ('Comparison of correlations for h/d=1')

legend('Simulation data','Reg-Int.Met h/d=1','Petera- Nu/Pr^1^/^3 =
0.101 Rem^0^.^6^8','Petera et al, h/d=1, Nu/Pr^1^/^3 =0.041
Re^0^.^8^2^6 S^0^.^6^0^9 (h/d)^-^0^.^0^9^9','Calvopina Nu/Pr^1^/^3 =
0.002*Re^1^.^0^5^9');


figure(6)

loglog(Rem,Num_Pr(7,:),'xk', Rem,NuPrcor1(2,:),'k', Rem,NuPr1,'b-
+',Rem,NuPr4(2,:),'r-', 'MarkerFaceColor',[0 0 0]);

xlabel('Re_m')

ylabel('Nu/Pr^1^/^3')

grid on;

title ('Comparison of correlations for h/d=0.5')

legend('Simulation data','Reg-Int.Met h/d=0.5','Petera- Nu/Pr^1^/^3
= 0.101 Rem^0^.^6^8','Petera et al, h/d=0.5, Nu/Pr^1^/^3 =0.041
Re^0^.^8^2^6 S^0^.^6^0^9 (h/d)^-^0^.^0^9^9');


figure(7)

loglog(Rem,Num_Pr(10,:),'xk', Rem,NuPrcor1(3,:),'k', Rem,NuPr1,'b-
+', Rem,NuPr4(3,:),'r-', 'MarkerFaceColor',[0 0 0]);

xlabel('Re_m')

ylabel('Nu/Pr^1^/^3')

grid on;

title ('Comparison of correlations for h/d=0.25')

legend('Simulation data','Reg-Int.Met h/d=0.25','Petera- Nu/Pr^1^/^3
   = 0.101 Rem^0^.^6^8','Petera et al, h/d=0.25, Nu/Pr^1^/^3 =0.041
   Re^0^.^8^2^6 S^0^.^6^0^9 (h/d)^-^0^.^0^9^9');
```